Global-scale Observations of the Limb and Disk (GOLD)

Release Notes

Revision 4.5 – August 5, 2022

Changes

Revision	Date	Changes
1.0	2/28/2019	Initial release
1.1	5/14/2019	Added "Incorrect Radiance values for the Night observations" to Known Issues
2.0	6/3/2019	Fixed issue with L1C NI1 data product and updated L1C NI1 and L1D NI1 to version 02.
		Initial limited release of Level 2 data products.
3.0	9/16/2019	New version of all L1C products with flatfield correction applied. Improved background subtraction algorithm for L1C OCC product.
		Release of additional L2 data products: TDISK, ON2, TLIMB and O2DEN through Aug 13, 2019 (with some exceptions, as noted below). QEUV through Jan 31, 2019.
3.1	12/6/2019	Added L1C and L1D Channel B NI1 data products to released products. See updated section 3.1.5 for more details.
		Added additional sections to Level 1 known issues: 3.1.12 No High Particle Background Flag 3.1.13 Incorrect Background Subtraction in Day and Night Scans 3.1.14 Incorrect variable names and units in L1C occultation files 3.1.15 Irradiance values in L1C occultation files are too large
3.2	4/8/2020	Added L2 NMAX data product to released products. Updated L2 TLIMB product to version 03.
		Added additional sections to Level 2 known issues: 3.2.4.5 Look up table constraints (ON2) 3.2.4.7 Flat Field correction artifacts (ON2)

		3.2.5.5 Flat Field correction artifacts (QEUV) 3.2.6 Issues with NMAX data
3.3	4/16/2020	Updated section 3.2.6 Issues with NMAX data
3.4	8/28/2020	Added additional sections to Level 1 known issues: 3.1.16 Field emission type events 3.1.17 Effect of stars on the brightness Added additional section to Level 2 known issues: 3.2.6.1 Model uncertainty (NMAX)
3.5	9/22/2020	Added additional image to Figure 3-10 Added additional gaps in data for TDISK (3.2.3.7), ON2 (3.2.4.6), and NMAX (3.2.6.1).
3.6	10/22/2020	Added additional gaps in data for TDISK (3.2.3.7), ON2 (3.2.4.6), and NMAX (3.2.6.1).
3.7	11/19/2020	Added additional gaps in data for ON2 (3.2.4.6) and NMAX (3.2.6.1) Added additional sections to known issues: 3.1.18 Horizontal artifacts in CHB NI1 scans 3.2.6.3 Flat Field correction artifacts (NMAX)
3.8	11/24/2020	Updated known issues: 3.1.4 Flatfield correction 3.2.4.7 Flat Field correction artifacts (ON2)
4.0	4/2/2021	New versions of all L1C and L2 data products Updated “Known Issues” based on latest data
4.1	6/24/2021	Added additional GYM actuation dates to Table 3-1 Updated section 3.1.17 Added additional section to Level 1 known issues: 3.1.22 Vertical depletion artifacts in NI1 data
4.2	9/14/2021	Added additional GYM actuation date to Table 3-1 Updated figures 3-21, 3-22, and 3-24 Added additional section to L2 known issues: 3.2.6.3 Vertical Depletion Artifacts (NMAX)

4.3	9/27/2021	Updated sections 2 and 3.1.1 with information regarding changes to the Channel A observation cadence. Updated figures 3-21, 3-22, and 3-24
4.4	11/17/2021	Added additional GYM actuation date to Table 3-1 Updated Level 2 O2DEN product to version 04 (see section 2.2.6)
4.5	8/5/2022	Added additional GYM actuation date to Table 3-1 Updated Level 2 TDISK product to version 04 (see sections 2.2.3, 2.2.7, and 3.2.3)

Table of Contents

1 Data Products:

This release includes a new version of all Level 1C (L1C) and Level 2 (L2) data products. Table 1-1 below provides the list of Version and Revision numbers associated with each data product for this release. The released dates of current GOLD data products can be found at https://gold.cs.ucf.edu/data/current-data-product-versions/

We refer users of these data products to the "***GOLD Science Data Product Guide***", available at https://gold.cs.ucf.edu/documentation/ for details about how these were obtained, about their file format and content.

Data Product	Version Number	Revision Number
L1C: DAY	03	01 and 02*
L1C: LIM	03	01 and 02*
L1C: OCC	03	01 and 02*
L1C: NI1	04	01 and 02*
L1D: DAY	03	01 and 02*
L1D: LIM	03	01 and 02*
L1D: OCC	03	01 and 02*
L1D: NI1	04	01 and 02*
L2: NMAX	02	01 and 02*
L2: O2DEN	04	01 and 02*
L2: ON2	03	01 and 02*
L2: QEUV	02	01 and 02*
L2: TDISK	04	01 and 02*
L2: TLIMB	04	01 and 02*

Table 1-1 Version/Revision Numbers by Data Product for this Release

*Note: For the period 2020/345 – 2021/046, all L1C and L1D data for Channel A and all L2 data are designated by revision 02. See section 2.1.1 for details.

2 Updates with This Release:

This release combines a full reprocess of all Level 1C and Level 2 data products. The Level 1 changes include updated radiometric calibration and an updated background subtraction, as well as several other changes described in section 2.1. All Level 2 data products were reprocessed using this new version of L1C data. This version also uses improved algorithms for the ON2, QEUV and TDISK data products, as described in section 2.2.

Update – 9/27/2021: The daytime, full-disk imaging cadence of GOLD was decreased on 9/6/21 to extend the instrument's capability to provide observations of the atomic oxygen 135.6 nm emissions, which are essential to three Level 2 data products: NMAX (in the nighttime ionosphere), ON2 and QEUV (both on the dayside). See section 3.1.1 for additional details.

Update – 11/17/2021: Updated L2 O2DEN data product to version 04. See section 2.2.6 for details.

Update – 8/5/2022: Updated L2 TDISK data product to version 04. See sections 2.2.3, 2.2.7, and 3.2.3 for details.

2.1 Level 1

2.1.1 Updated Filtering of Photon Events by Pulse Height

The GOLD detectors employ a z-stack of microchannel plates that convert single photoelectrons produced at their respective spectrograph focal planes into pulses with a gain of ~ 10^7 electrons that are detected by their electronics packages (McClintock et al., 2020a and 2020b). The size of the pulse, referred to here as 'pulse height', is recorded by the electronics for each detected photoevent. The pulse height filtering window has been modified for this release such that all events with a pulse height value of 0, 1, 2 or greater than 200 are filtered out. This update filters out many more energetic-particle-produced events, which typically have higher pulse height values than events produced by photons. The result is a reduction in mislocated events that tend to cause a horizontal stripe across the detector when high particle backgrounds are present. McClintock et al. 2020a describe the particle backgrounds distributions and morphologies.

During the period 2020/245 to 2021/046, the Channel A detector was being run at very high gain due to advanced degradation at the 135.6 nm line. As a result, the pulse heights of normal photon events were increased significantly, and the pulse heights of ~20% of normal photon events were shifted beyond the new filter level of 200. To ensure that these normal photon events are not excluded, we used the previous version of lower-level data (with a lower pulse height filter level) when processing the L1C Channel A data during that date range. In order to emphasize this difference, all L1C and L1D data (Channel A) and all L2 data from 2020/245 to 2021/046 are designated as revision '02'.

2.1.2 Time-dependent Background Subtraction

In previously released versions of L1C data, the presence of rapidly varying particle background levels was noted. This new correction uses unilluminated areas of the detector to measure the background rate for each two-second L1B detector image. The approximate background rate is used to scale a reference dark image which is subtracted from each L1B image before L1C binning occurs. This processing is only applied to DAY, LIM, and NI1 observations.

2.1.3 High Particle Background Flag

A flag indicating the presence of high particle background levels during an observation has been added as a global attribute named "High_Background" in DAY, LIM, and NI1 L1C files.

2.1.4 Update to Radiometric Calibration

The radiometric calibration has been updated for both the Channel A and Channel B instruments based on new, unpublished analysis performed in June 2020. This was accomplished by generating new instrument detection efficiency functions for each channel. It should be noted that in previous releases, the Channel A and Channel B instruments both used the same detection efficiency, which was applied to every row of the detector along the spectrograph entrance slit. They now each have a unique curve. A comparison of the previous combined detection efficiency curve to the new curves is shown in Figure 2-1. These apply to the center of the field of view.

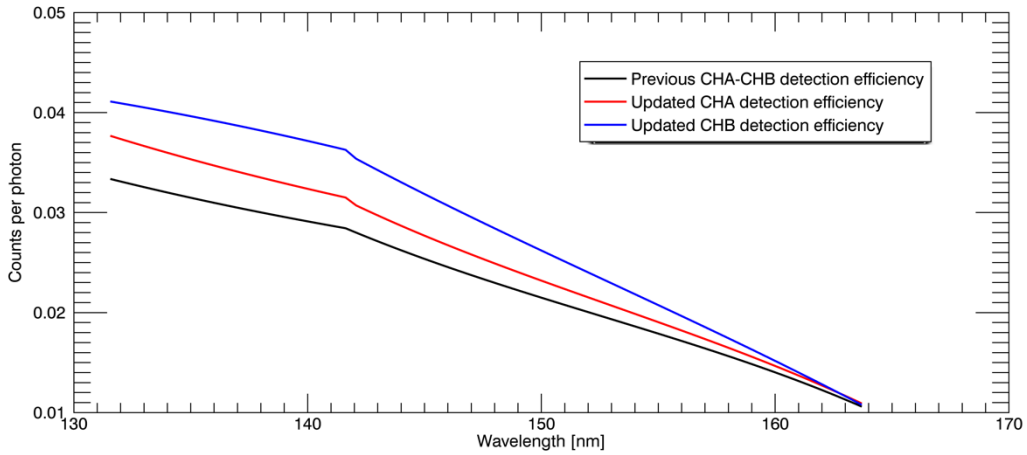

Figure 2-1 detection efficiency at the center of each channel's field of view

2.1.5 2D Detection Efficiency Function

In past releases, a single instrument detection efficiency (black curve in Figure 2-1) was applied across the entire field of view (length of the spectrograph entrance slit). In this release, a time dependent two-dimensional detection efficiency has been applied to Channel A data. At this time, a single, updated curve (blue line in Figure 2-1) appears to adequately describe the CHB detection efficiency along its entire field of view.

2.1.6 Corrected Calculation of L1C Uncertainties

This release includes a correction to how the uncertainties in the L1C products are computed. The affected L1C variables are Corrected_Count_Systematic_Unc, Corrected_Count_Random_Unc, Radiance_Random_Unc, Irradiance_Systematic_Unc, and Irradiance_Random_Unc.

See section 3.1.21 regarding a known issue with Radiance_Systematic_Unc.

2.1.7 Radiance values for wavelengths less than 135.0 nm have been set to NaN

Due to the loss in detector gain over time (see above) flatfield correction introduces artifacts at wavelengths less than 135.0 nm; therefore, all radiance and associated uncertainty values below 135.0 nm have been set to NaN values. Detector counts at these wavelengths are still reported in the L1C data files. These should be used with caution.

2.1.8 Change Occultation Variable Names

All variable names in the L1C OCC files previously containing “Radiance” have been corrected to use “Irradiance”.

2.1.9 Corrected Irradiance Values in L1C Occultation Files

In the previous release, irradiance values (but named radiance in previous releases) in the L1C OCC netCDF files were too large by a factor of 1.88. This issue has been fixed in this release.

2.1.10 L1C File Size Increase

The Level 1C files in the latest reprocessing have become substantially larger. This is attributed to the reduced compressibility of the data stored in several of the variables within these files.

2.2 Level 2

2.2.1 Use of updated L1C data products

All L2 data products have been reprocessed from the updated L1C data. This produces an updated version number for all products whether or not the Level 2 algorithms for each product have changed since the previous version. In many cases, particularly the dayside and nightside disk data products (ON2, TDISK and NMAX), improvements in the L1C processing have helped to fix the artifacts seen in previous versions of these products. In addition, changes to the GOLD instrument calibration incorporated in this reprocessing result in an overall decrease in the L1C spectral radiances (see section 2.1.4). This change propagates directly into those L2 data products that depend directly on absolute radiances, specifically ON2, QEUV and NMAX. Since the calibration change is largest at shorter wavelengths, the oxygen 1356 radiances changed more than the integrated N_2 LBH.

All Level 2 data in the current release other than NMAX are derived from Level 1C Channel A data only. Both Channel A and B NI1 L1C data are used to derive the NMAX data product.

2.2.2 ON2 algorithm improvements

In previous releases of this data product the algorithm operated directly on each valid L1C DAY pixel and therefore the spatial sampling and resolution of the final ON2 data product was identical to the input L1C (125 x 125 km^2 at satellite nadir). To increase signal-to-noise and improve the precision of the ON2 product the v03 retrievals now bin the input L1C radiance using a 2x2 binning algorithm. As a result, the v03 ON2 product is output at a lower spatial resolution of 250 x 250 km^2. This still meets the Level 1 requirements on spatial resolution for this data product. Previous versions exceeded the requirement, but at the cost of poorer retrieval precision.

Additional improvements to the ON2 algorithm include changes to the spectral bandpass used to define both the oxygen 135.6 nm and N_2 LBH bands used by the algorithm. These changes were made to improve the signal-to-noise in the integrated radiances, and to avoid spectral features that were susceptible to long-term instrument degradation and trends.

2.2.3 TDISK algorithm improvements (updated 8/5/2022)

The update of the TDISK data product to v04 includes several significant changes to the TDISK algorithm, including:

- The GOLD instrument model used in the TDISK retrieval algorithm has been expanded to include a 2-dimensional point spread function (PSF). The PSF describes the instrument response, which was previously only characterized along the spectral dimension. The second dimension introduced in v04 characterizes the instrument response in the spatial dimension, along the GOLD entrance slit. This fixes some known biases that were caused by changing instrument performance, e.g., spectral resolution, along the slit, which corresponds to the latitudinal gradient in GOLD data.
- Spectral binning is now performed on the input L1C DAY radiance spectrum before applying the Level 2 retrieval algorithm. This is in addition to the 2x2 spatial binning that was introduced in v03 processing. The spatial binning is done first, followed by spectral binning. The 800-element counts spectrum for each 2x2 binned L1C super pixel (0.04 nm spectral binning) is binned by a factor of four to yield a 200-element counts spectrum (0.16 nm resolution), which is then passed in to the L2 retrieval algorithm.
- Retrieval of a wavelength stretch parameter, which was active in previous versions, has been turned off in v04. This instrument effect is now known to be small and so can be neglected. Users should note that the WAVELENGTH_STRETCH parameter has been retained in the Level 2 TDISK data files, with all elements set to NaN. The wavelength shift parameter is still retrieved in v04.
- The LBH band relative vibrational populations are held fixed as in v03 but the full seven-element VIBRATIONAL_POPULATIONS vector is still output to the Level 2 files. The first element of this array is a retrieved scale factor that is used to adjust the absolute

brightness of the forward model LBH spectrum to match the observed spectrum for each pixel.

2.2.4 QEUV algorithm improvements

The QEUV algorithm was modified to use new spectral bandpass definitions for the oxygen 1356 and LBH radiances, consistent with the ON2 algorithm changes described in section 2.2.2.

2.2.5 Edge filtering in ON2 and TDISK binning

The pixels at the equatorward edge of an L1C DAY scan (i.e., the southernmost valid pixel for a North hemisphere scan and northernmost valid pixel for a South hemisphere scan) often demonstrate anomalous values or an increase in noise due to the reduced number of valid L1B pixels available to be coadded for those L1C pixels. Therefore, before L1C DAY data is binned for the ON2 and TDISK algorithms an edge filter is applied that identifies these edge pixels and sets them to NaN.

2.2.6 O2DEN array dimension changes (updated 11/17/2021)

As of 11/17/2021, the L2 O2DEN dataset has been updated to v04. Users should be aware that the actual values of the O2DEN data product – altitude profiles of O_2 number density – are identical in v04 compared to v03 because nothing has changed in the underlying Level 2 O2DEN algorithm.

The only changes made in v04 are in the format of the Level 2 data files, specifically the dimensions of the output altitude arrays. Both the retrieval altitude grid (ZRET) and the input data altitude grid (ZDAT) are now fixed arrays of static size, rather than having a different size and range for each occultation event as in the v03 dataset.

Specifically, ZRET is now a REAL 31-element grid ranging from 100 to 250 km (NZRET=31), while ZDAT is a 27-element grid from 104 to 300 km (NZDAT=27). Grid points outside the range of either the input transmission data or retrieved O_2 profiles, and associated quantities, are populated with fill values.

2.2.7 Summary of changes in Level 2 data products

The GOLD Level 2 data products reprocessed for this release differ from the previous data versions to various degrees, depending on their sensitivity to underlying L1C changes and whether or not the L2 algorithms have been improved. This section provides a high-level summary of the changes that users can expect to see in each L2 data product.

ON2:

On average the v03 ON2 is ~5% higher than v02. This change is due to a combination of L1C calibration changes and new definitions of the oxygen 135.6 nm and N_2 LBH spectral bandpass used in the L2 algorithm. The addition of 2x2 spatial binning in the v03 algorithm reduces retrieval random errors.

TDISK (updated 8/5/2022):

There are significant changes in the v04 TDISK retrievals compared to v03. Overall, the v04 temperatures are hotter than v03, but the difference varies depending on multiple factors, including latitude, signal to noise in the binned L1C spectra, and solar zenith angle (or local time).

The v04 algorithm improvements reduce or eliminate a number of artifacts that were present in the v03 data. These include: 1) a cold temperature bias in low signal-to-noise (SNR) regimes (high solar zenith angles, low solar activity), 2) biases in latitudinal gradients, maximizing at the equator, due to along-slit gradients in instrument spectral resolution, 3) residual TDISK dependence on measurement geometry (e.g., emission angle), and 4) sensitivity of the TDISK retrieval to particle background conditions at the satellite. Examples of these improvements are shown in the plots below.

Figure 2-2 shows a top-level summary of temperature changes for the entire GOLD mission to date. The v04 temperatures are ~50-100 K hotter on average from the beginning of the mission through the end of 2021. The two versions tend to converge beginning in 2022. A more detailed comparison is shown in Figure 2-3 in terms of 10^{o} x 10^{o} (LAT/LON) binned data at multiple latitudes. This plot shows how the maximum deviations in the two versions tend to occur early in the GOLD mission, and in the wintertime in both hemispheres, particularly at high latitudes. These times correlate with higher solar zenith angles and/or lower solar activity, and hence with lower SNR data. Defining a (somewhat arbitrary) SNR threshold of 40 it is clear that when SNR exceeds this threshold, indicated by the black symbols, differences between the versions are small. This is a clear indication of the cold bias in the v03 data at low SNR, which is largely fixed in v04.

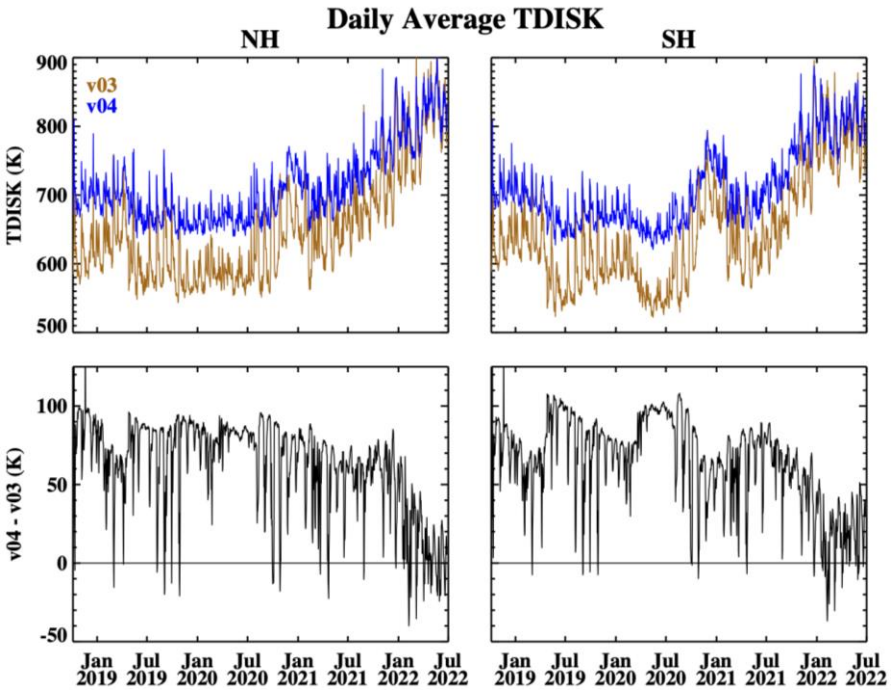

Figure 2-2 Daily average v03 and v04 TDISK in the top row, and the difference in the bottom row. Data from the Northern and Southern hemisphere scans are shown in the left and right columns, respectively.

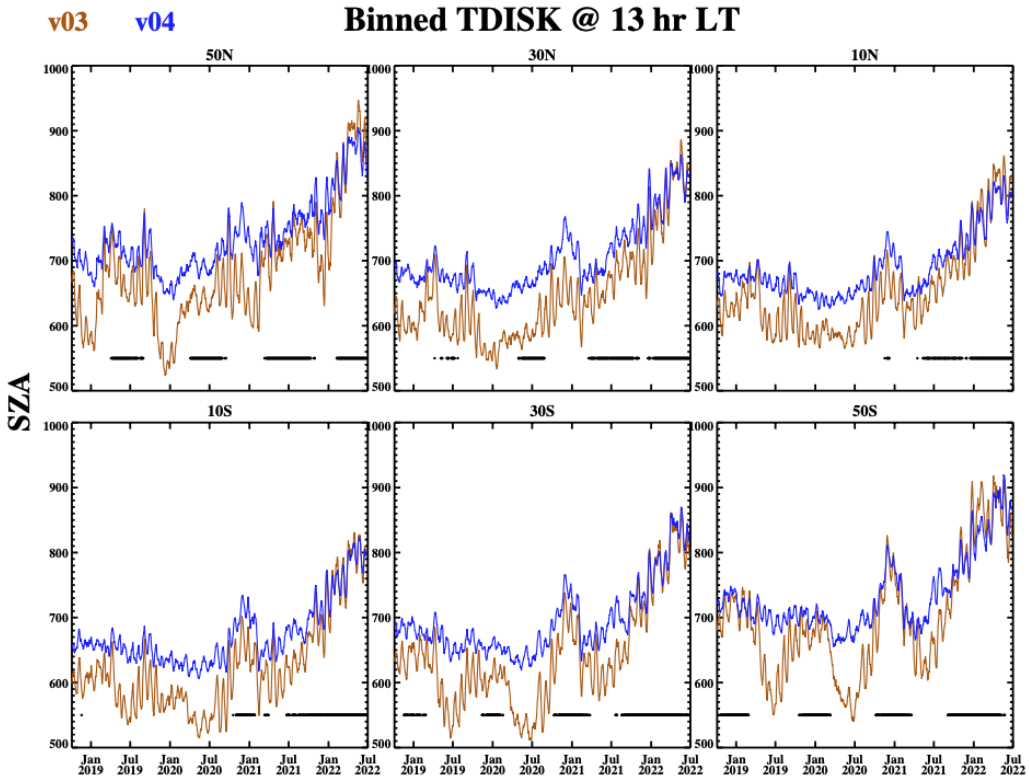

Figure 2-3 Comparison of v03 and v04 TDISK at different latitudes from 50N to 50S. Local time is fixed at 13 hours. Black dots along the bottom indicate days where the mean signal-to-noise is 40 or higher.

It was well-known that previous versions of TDISK data contained artifacts in the latitude gradient of the temperature. This was caused by real changes in instrument response along the GOLD slit, which is aligned vertically, along the latitudinal direction. Previous retrieval versions did not account for these instrument effects, but v04 does with the inclusion of the 2D PSF. The most obvious manifestation of this artifact was a bias in temperatures retrieved at the equator from back-to-back Northern hemisphere (NH) and Southern hemisphere (SH) scans. These retrievals are co-located spatially and separated by only ~12 minutes in time, so geophysically they are expected to agree on average within retrieval noise. However, the equator is sampled from opposite ends of the GOLD slit in NH compared to the SH scans, so along-slit gradients are maximized in this scenario. A consistent NH/SH bias of ~40K was always seen in v03 data. Figure 2-4 shows a comparison of this NH/SH bias for the two data versions. It's clear that in v04 data this bias, while not completely eliminated, is significantly reduced. On average it is < 20K and therefore well below the mean random retrieval errors. The latitudinal gradients overall in v04 data are much smoother and more realistic than in v03 (not shown).

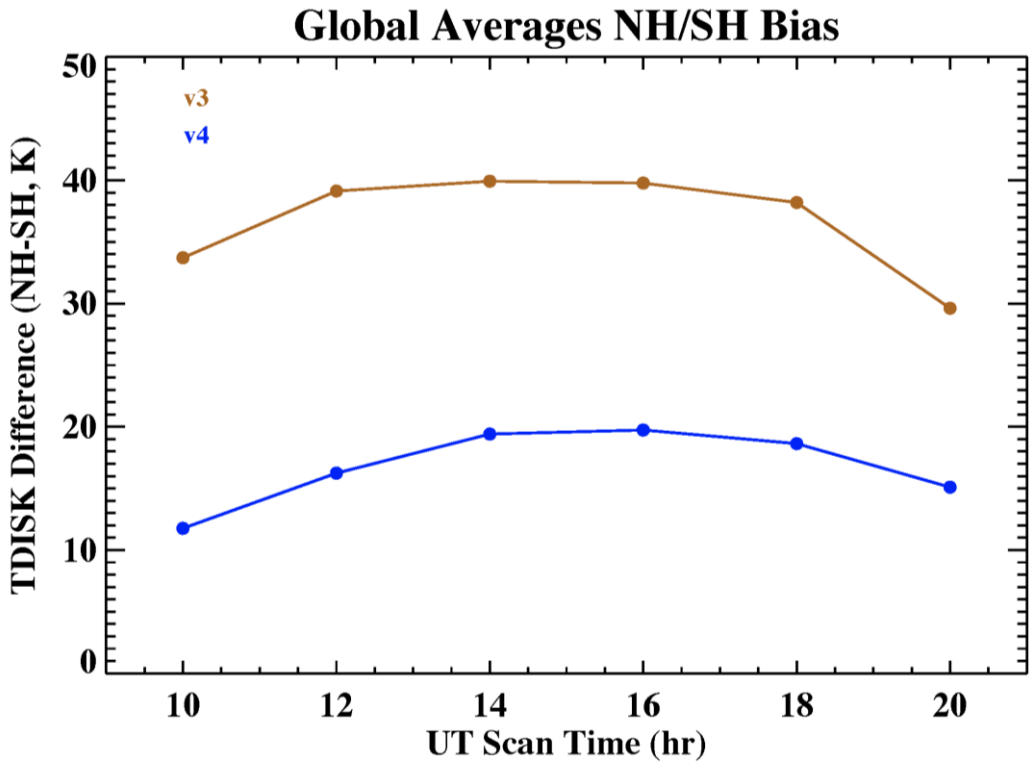

Figure 2-4 Difference in TDISK values retrieved at the equator from sequential Northern and Southern hemisphere (NH/SH) scans. These values are calculated from a mean over the entire data set and plotted as a function of the UT scan time during the day. Brown and blue curves are for v03 and v04, respectively.

Another artifact that was observed in previous versions was a positive correlation in retrieved TDISK values with increasing emission angle (EMA) of the measurement. EMA is defined as the angle, relative to local zenith, of the look vector from GOLD to the 150-km emission point of the measurement location. It is a measure of the magnitude of the off-nadir view angle, and increases radially in all directions away from the sub-satellite point. Increased EMA corresponds to longer path-lengths to the emission point, and thus increased brightness in the path-integrated LBH spectrum. Retrieved geophysical parameters should be independent of this measurement geometry. As Figure 2-5 shows, the v03 TDISK retrievals were positively correlated with EMA, with increases of up to ~50K at high EMA in pixels close to the edge of the observable disk. This bias remains in v04, but it is very much reduced to ~10K at maximum, which is well within the retrieval random errors.

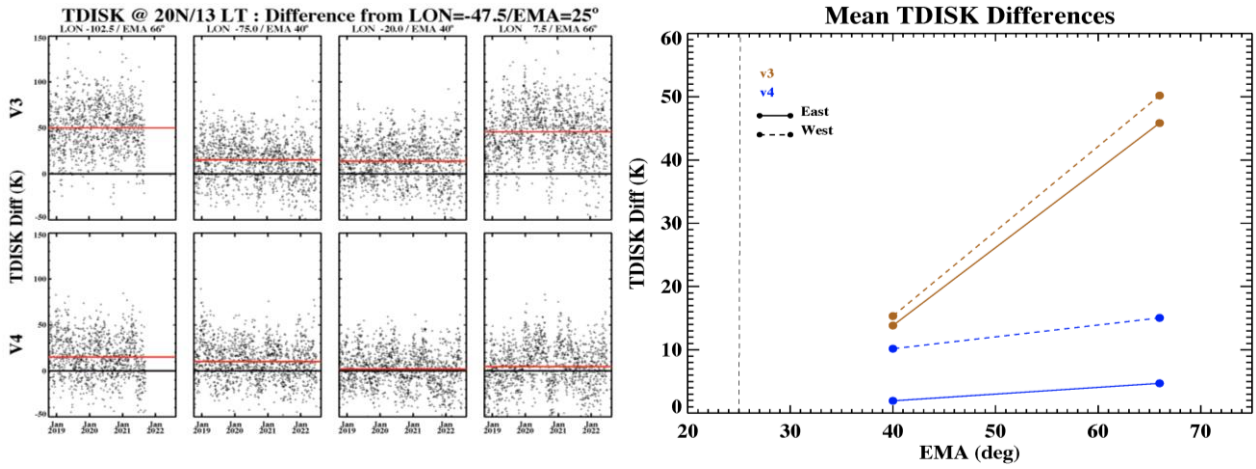

Figure 2-5 Difference in TDISK values retrieved at the same latitude (20N) and local time (13 hr) but different longitudes. The left panel shows the difference in TDISK values retrieved in longitude bins separated by 27.5° and 55°, relative to sub-satellite longitude. These bins differ significantly in the emission angle (EMA) of the measurement. V03/v04 data are shown in the top/bottom rows. The right panel shows the mean differences over the entire data set, plotted as a function of EMA.

Version 03 TDISK was known to exhibit a hot bias during periods of high ambient particle background at the satellite. This is illustrated in the left column of Figure 2-6, which shows retrieved TDISK values plotted against the particle background level. This plot only includes data from days with low solar and geomagnetic activity in 2019. It is clear that v03 TDISK retrievals during high background conditions are hot compared to low background conditions. The blue line is a simple linear fit to the data, with the linear coefficient value printed in the lower right corner of the plot. The corresponding plots with v04 data are shown in the right column. It is clear that most of the correlation with particle background has been removed, and the linear fit coefficient is reduced by a factor of ~3.

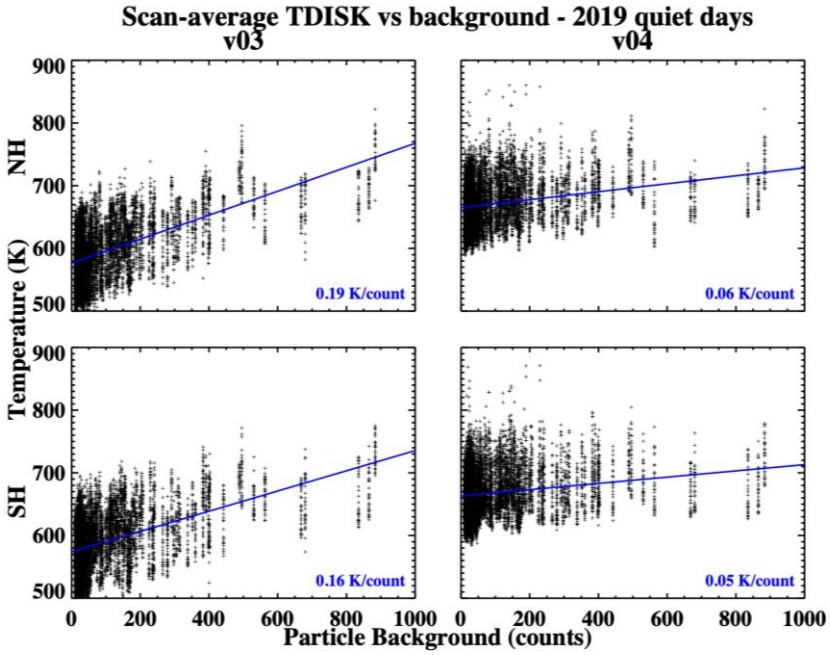

Figure 2-6 Scan averaged TDISK values plotted as a function of particle background, using data from days with low solar and geomagnetic activity in 2019. Top(bottom) rows show data from the NH(SH) scans, while the left and right columns correspond to v03 and v04, respectively. The blue line in each panel is a simple linear fit to the data, with the value of the linear term provided in the bottom right.

QEUV:

The v02 QEUV values are lower than v01 by ~10% on average. As with ON2, the change is due to a combination of L1C calibration changes and the new definitions of oxygen 135.6 nm and N_2 LBH spectral bandpass used in the L2 algorithm.

TLIMB:

There are minimal changes in v04 TLIMB compared to v03, with v04 ~2-5K colder on average. Larger differences of up to 20K occur at times of peak particle background levels, which is probably due to the improved background removal in the new L1C data minimizing artifacts in the TLIMB retrievals.

O2DEN:

Very minor changes are seen in the v04 data compared to v02. Mean changes over the data set are less than 2% at all altitudes. These are entirely due to differences in the underlying L1C OCC data, as there were no changes to the L2 O2DEN algorithm in v04 (or v03 before it). The only differences between v04 and v03 are changes to some array dimensions as described in section 2.2.6.

NMAX:

The v02 NMAX values are decreased by ~10% on average compared to v01. These differences are entirely due to the L1C calibration changes at 135.6 nm, as there were no changes to the L2 NMAX algorithm.

3 Known issues:

There are a number of known issues with the data provided in this and previous releases. This section provides a description of these issues and guidance to the user community on the use and interpretation of GOLD data products. This documentation is cumulative so that descriptions of known issues will remain until they are resolved in future releases. For the current release, Section 3.1 describes known issues with Level 1 data while Section 3.2 describes known issues with the Level 2 data.

3.1 Level 1

3.1.1 Detector "burn-in"

The GOLD detectors employ a z-stack of microchannel plates that convert single photoelectrons produced at their respective spectrograph focal planes into pulses with a gain of ~ 10^7 electrons that are detected by their electronics packages (McClintock et al., 2020a and 2020b). The size of the pulse, referred to here as 'pulse height', is recorded by the electronics for each detected photoevent. As the detectors accumulate events, pulse height declines, a process that we refer to as 'burn-in'. This primarily affects emissions produced by the OI 135.6 nm doublet and is mitigated by using an internal stimulus lamp to obtain a 'flat field image' that is used to remove burn-in. As the gain continues to decline, errors introduced by the flat field process can become unacceptably large (as occurred during the first year of the mission). Before that point, a mechanism (Grating Yaw Mechanism – GYM) within the affected spectrograph is actuated to rotate the grating, placing the spectrum on a different location on the detector. At the beginning of the mission, the doublet was placed at the edge of each detector's active area. The GYM mechanisms have been actuated from time to time as summarized in Table 3-1. Each actuation moves the spectrum to longer wavelengths by approximately 0.8 nm (~ 20 L1C detector pixels). Because Channel B observes only during the night, the fluence of photons is much smaller than that for Channel A and its GYM has been actuated fewer times.

Detector GYM Actuation Dates	
Channel A	**Channel B**
4/26/2019	3/14/2019
10/10/2019	10/20/2020
3/20/2020	6/1/2021
8/11/2020	11/11/2021
2/8/2021	5/3/2022
6/12/2021	
8/27/2021	

Table 3-1 Detector GYM Actuation Dates

Daytime airglow emissions are the dominant contributor to the total fluence of 135.6 nm photons and therefore to sensitivity decline at 135.6 nm. Because the useful range of motion for the GYM is limited, the cadence of Channel A daytime observations was reduced beginning on 9/6/21 in order to extend production of the 135.6 nm-dependent Level 2 data products (NMAX, ON2, QEUV). In addition, stellar occultation observations are now being restricted to nightside occultations only. Changes in the spatial coverage of daytime observations can also contribute to extension of observations, and a final choice for the tradeoff between temporal cadence and spatial coverage is yet to be completed.

3.1.2 Gradient in sensitivity from top to bottom of detector

In previous releases, we did not correct for changes in the Channel A instrument sensitivity over the field of view (along the spectrograph entrance slit). This effect can be as large as ~20% from top to bottom of the slit.

Figure 3-1 shows vertical slices of detected counts taken at the sub-spacecraft longitude for successive north-south scans near 12:00 local time (LT). In the top panel, labeled ‘Ch A Vertical Cuts for O’, near the equator, where the top and bottom of the slit overlap on successive scan swaths, the count values for O 135.6 nm (as well as radiance values in the L1C data files) extracted from the southern hemisphere scan (red) are ~10% larger than those from the northern hemisphere scan (black). This led to ‘banding’ at the equator in the OI images of the entire disk. The magnitude of the difference (and the level of banding) decreases with increasing wavelength as illustrated by the extracted LBH counts shown in the lower panel.

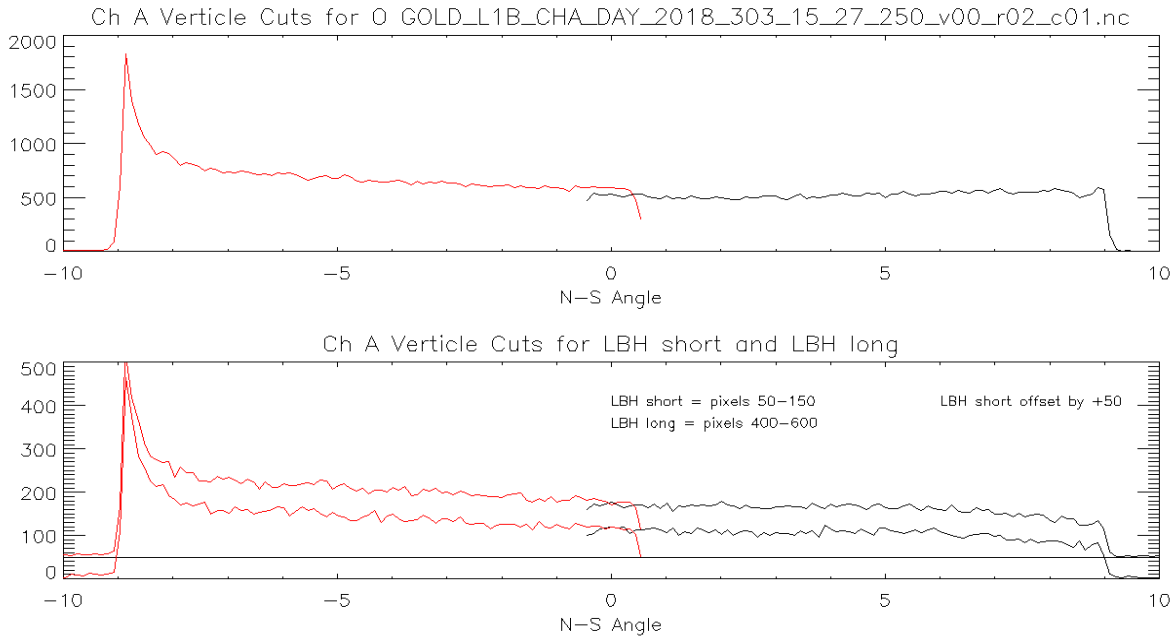

Figure 3-1 Uncorrected Vertical Sensitivity Variation

In this release, application of a 2-dimensional sensitivity function (Section 2.1.5) to Channel A has reduced the magnitude of this effect but has not entirely eliminated it. The left six panels in Figure 3-2 plot the percent difference (southern hemisphere – northern hemisphere) of 135.6 nm emissions at 6 UT scan times during the day over the course of the mission. These differences are calculated from data averaged in a 10^{0} x 10^{0} (latitude x longitude) bin centered at the equator and the sub-satellite longitude. Vertical blue lines mark the days when the grating GYM was actuated. Large differences for times after 12:00 LT, present just before the first two actuations and just after the second one, result from severe detector burn in that could not be adequately corrected by the flat field algorithm. Differences in total LBH emission are plotted in the right six panels. Although these plots show little evidence for detector-gain induced artifacts, there appears to be an overall ~ 10% decline that most likely results from residual errors in the 2-D sensitivity function for longer wavelengths. This trend is not observed in the 2-D sensitivity for OI 135.6nm.

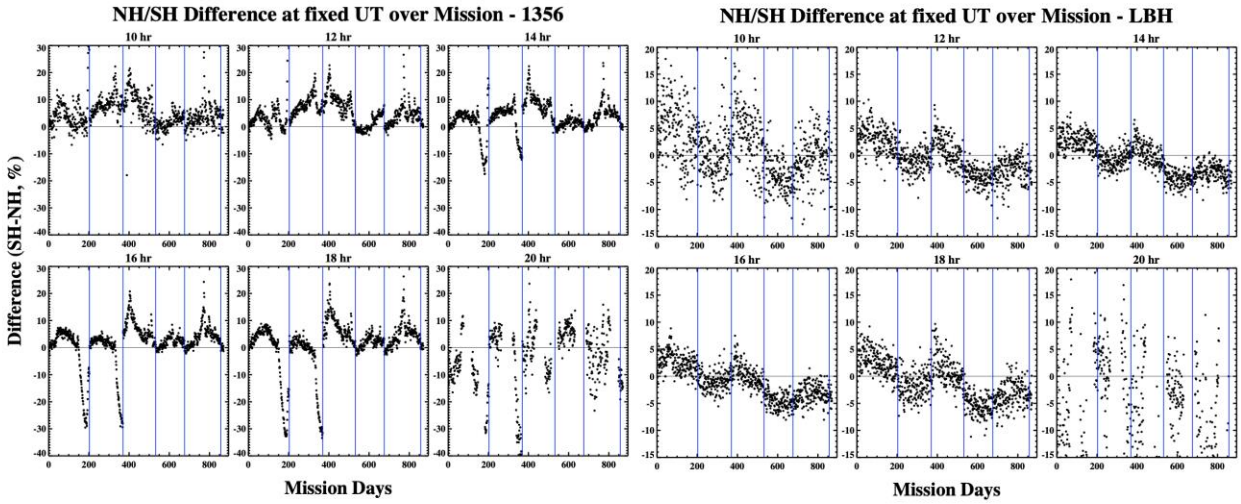

Figure 3-2 Percent differences (southern hemisphere – northern hemisphere) in OI 135.6nm (left six panels) and in total LBH (right six panels) for 6 times during the day throughout the mission.

3.1.3 Time Delay of Reconstructed Full Disk Images

The projected height of the slit covers slightly more than half the Earth, with an overlap around the equator when scanning the northern and the southern hemispheres. Not all banding observed in these overlapping scans is caused by residual errors in the instrument 2-dimensional sensitivity function (Section 3.1.2). Full disk images made by combining northern hemisphere radiance images with those from the adjacent (in time) southern hemisphere image, can also show banding because incidence and emission angles change throughout the 30 minutes during which the images are obtained. The effect is more pronounced early and late in the day. Figure 3-3 shows this effect on a sample DAY scan.

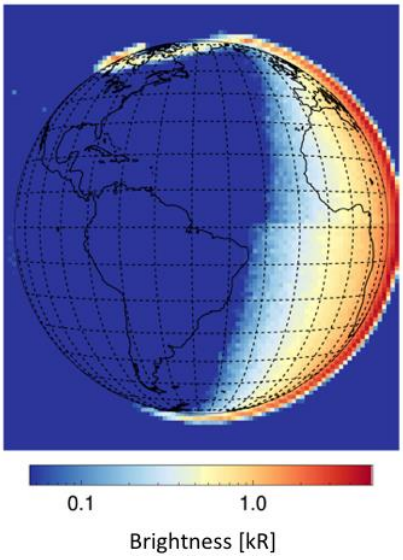

Figure 3-3 Combined scans of north and south latitudes from L1C data

3.1.4 Incomplete Scattered Light Correction

Due to the signal to noise limitations, the first version of the background and scattered light removal algorithm assumed that there is no wavelength dependence. This has not been corrected in the current release. Figure 3-4 shows that there is a small slope for regions of the spectrum < 138 nm that is not removed by the current processing.

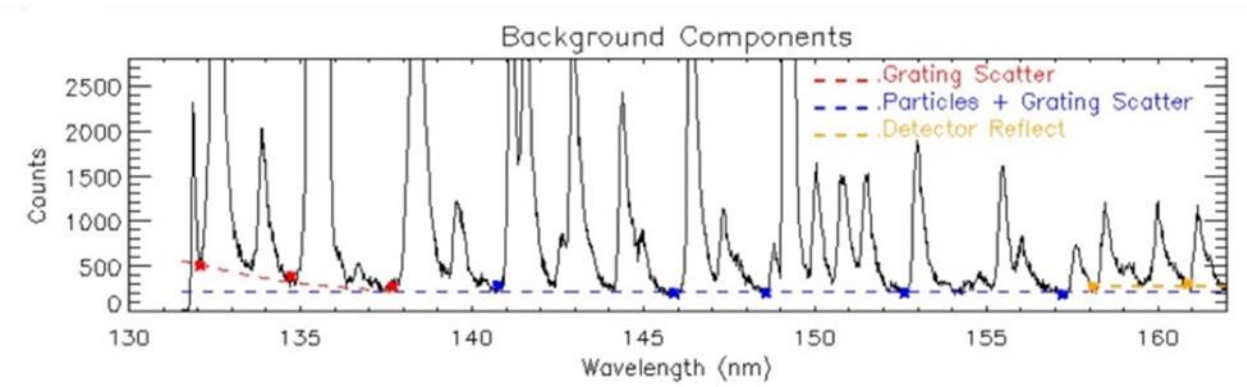

Figure 3-4 Wavelength Dependence Scattered Light

3.1.5 Flatfield Correction

The flatfield correction attempts to correct for a relative drop in detector sensitivity due to line burn-in. See the Public Science Data Products Guide (section 3.3.1.1) and McClintock et al., 2020b. The flatfield correction has some limitations. It is not always able to totally account for variations in detector gain that are caused by diurnal temperature variations in the instrument. The result is that the flatfield correction can under- or over-correct data, depending on the time of day and season. In addition, those parts of the slit that observe the aurora receive larger photon fluence and 'burn-in' more rapidly. These areas can be under-corrected. The error is largest for the brighter component of the 135.6 nm OI doublet and increases with 'burn-in', typically reaching maximum value just before a GYM actuation. This is particularly true for the first two GYM actuations (4/26/2019 and 10/10/2019). Figure 3-5 shows a simulation of the magnitude of the flatfield correction on the brightness of several emission features in the Channel A spectrum. These curves were produced by multiplying a model observed spectrum from the first days of the mission by the flat field images taken on the day of observation to produce a simulated spectrum with burn-in. The radiances extracted from the 'burn-in' images are then compared to those from the model observed spectrum to compute the magnitude of the correction for that day. Figure 3-6 shows the impact of the flat field correction errors on L1C DAY observations. An under-correction (left panel) of the 135.6 nm emission occurs for latitudes just south of the equator in a southern hemisphere scan approximately 1 month before a GYM actuation. This part of the slit observes the auroral region during northern hemisphere scans. Diurnal instrument temperature variations can sometimes result in an over-correction (right panel) of the 135.6 nm radiance.

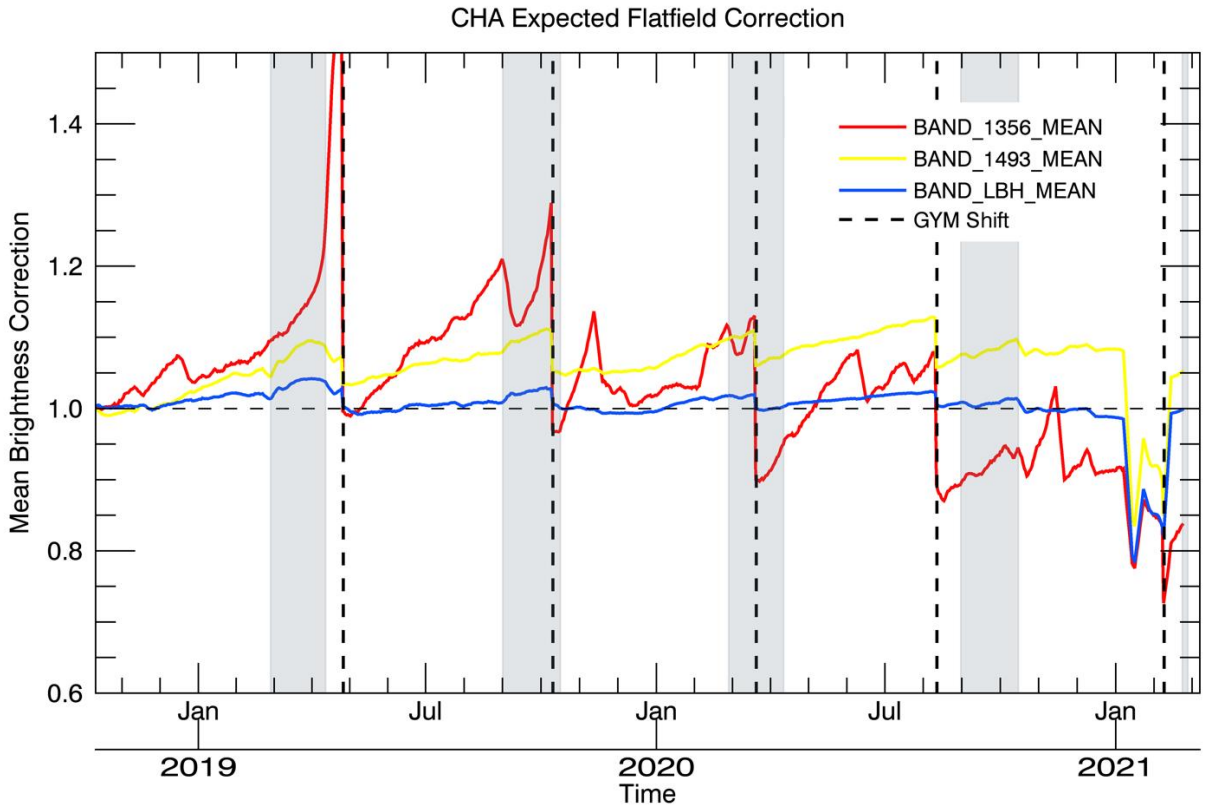

Figure 3-5 Channel A Expected Flatfield Correction. Vertical dashed lines and shaded areas denote GYM shift dates and period when the earth occults the sun during some part of a day.

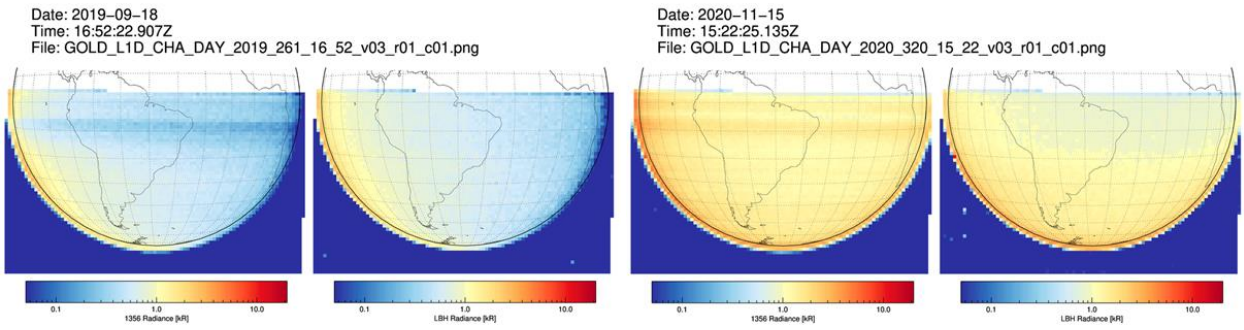

Figure 3-6 Effect of flat field correction errors on L1C DAY observations. The horizontal banding is the result of under-correction (left panel) or over-correction (right panel) of the 1356 radiance.

3.1.6 Limited Channel B Data

During the first three months of operations, the Channel B degradation (also referred to as 'burn-in') proceeded faster than expected. As a result, the 135.6 nm data became unreliable about December 15, 2018, but the GYM was not activated until March 15, 2019. Since then, the use of Channel B has been largely restricted to nighttime observations when the 135.6 nm emissions are an order of magnitude less than daytime emissions. As a result, the Channel B 135.6 nm radiance values reported after March 15, 2019 are reliable. Initial analysis of GOLD nighttime

data from Channel B during December 15 of 2018 to March 15 of 2019 indicates that the current version of the data from that period are useful for qualitative analysis but not for quantitative analyses. To avoid unintentional inclusion of the unreliable radiances in quantitative analyses, the nighttime data for that period are not included in the .tar files generated in searches for data on the GOLD website. However, the data for that period is available by request through a link on the GOLD data download page (https://gold.cs.ucf.edu/search).

For Channel B, only nighttime (NI1) data is currently available. Channel B has made most of GOLD's nighttime observations, and release of Channel B nighttime data were given priority over the Channel B daytime observations since Channel A provides the most comprehensive daytime coverage.

3.1.7 Slit Movement due to Thermal Changes

The projected image of the slit on the detector moves vertically ~ ± 2 L1B pixels with changing temperature throughout an orbit and throughout the year. We are currently using the "nominal" slit position on the detector to assign a latitude to every corresponding row along the slit and are not correcting for any movement of the image of the slit in that dimension (In contrast, the wavelength scale is determined from the position of the OI 136.6 nm doubles and NI 149.3 nm triplet atomic emissions for each L1C image). This effectively adds additional uncertainties in the assigned latitude. The image in Figure 3-7 traces the displacement of the bottom of the slit image relative to row 52 in each L1B spectral-spatial image as a function of universal time (UTC) and of season throughout a year. Typical range of motion throughout the day is ~ ±2 L1B pixels (~± 30 km in latitude at nadir) with comparable seasonal variation. This instrument effect will be corrected in a future release.

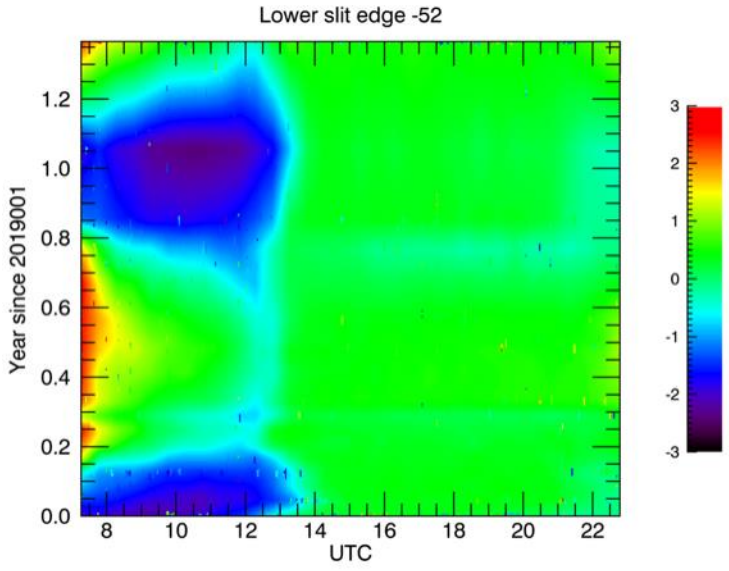

Figure 3-7 Vertical Slit Motion with Temperature measured in L1B pixels

3.1.8 Stellar Occultation Wavelength Feature

The wavelength determined during a stellar occultation is purely a function of the star within the occultation slit and so the solution is not applicable when the star is outside that field of view. For these time steps, the default high resolution slit wavelength solution is used. This adds an unrealistic discontinuity in the wavelength scale. This known displacement is present in this data release.

3.1.9 Incorrect Background Subtraction at Limb in Day Scans

The sharp transition in the background between On and Off Limb is not accurately captured, so the background is over corrected as seen in Figure 3-8. This will be addressed in future releases.

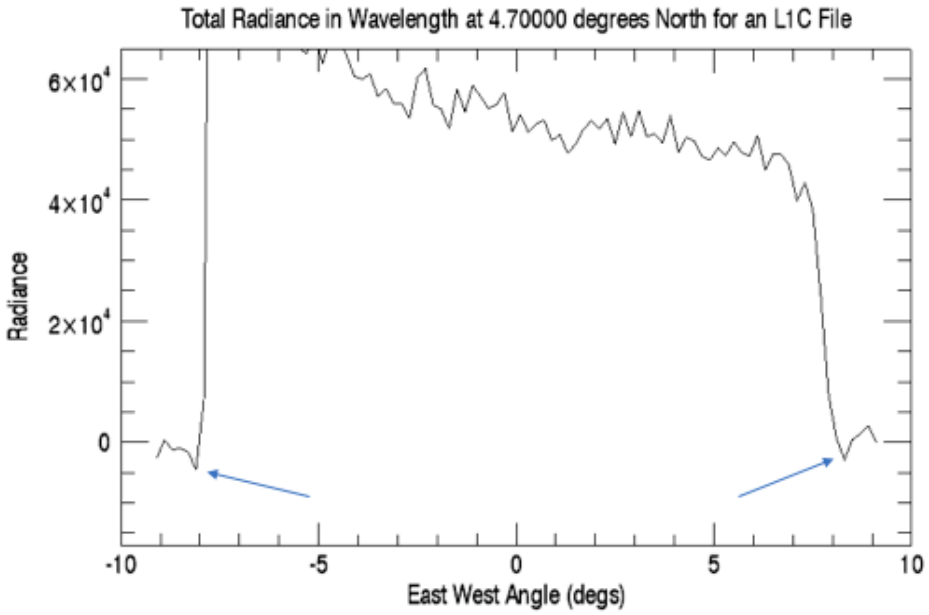

Figure 3-8 Over Corrected Background Subtraction at Limb

3.1.10 No local dead-time Correction for Occultations

Local dead-time correction, which affects the Occultations, has not been applied. The magnitude of the effect varies with the brightness of the star. A sample correction is shown in Figure 3-9.

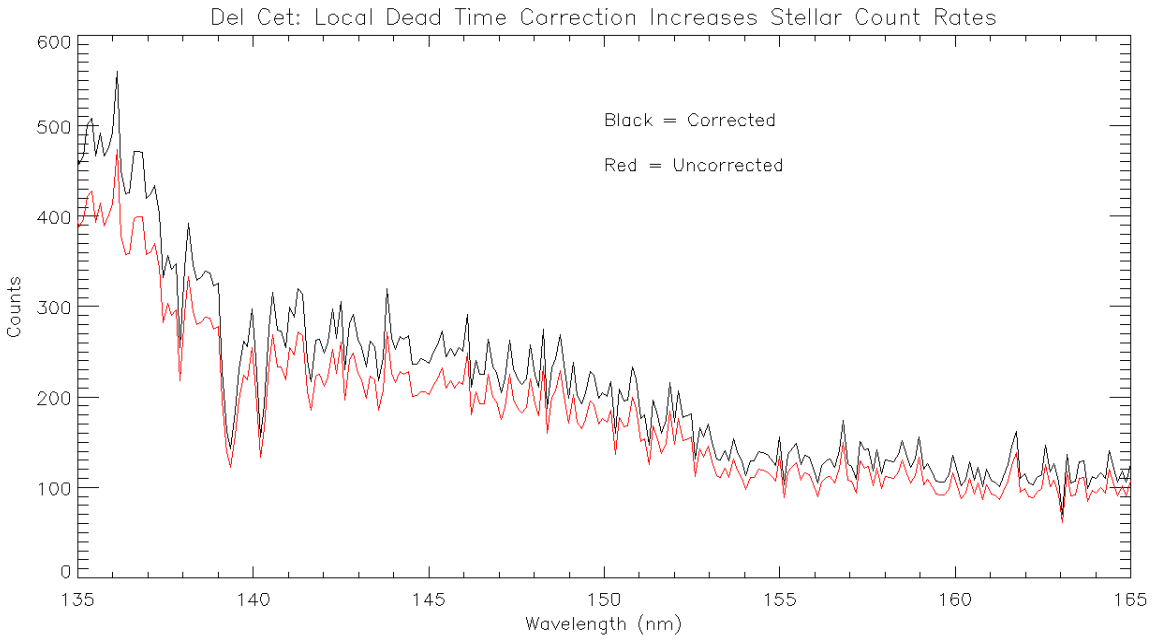

Figure 3-9 Counts Comparison with Dead-Time Correction

3.1.11 Variation in Spectral Resolution Along the Spectrograph Entrance Slit

The point spread function for GOLD spectra, which is well approximated by a Gaussian function, varies as a function of position along the slit and as a function of wavelength. Panels in Figure 3-10 are contour plots of PSF full-width-at-half-maximum (FWHM) for the southern hemisphere (rows 0 – 55) and northern hemisphere (rows 50 – 104) of L1C image cubes. PSF values are largest at the ends of the spectrograph entrance slit, which occurs for L1C row 55 in southern hemisphere scans (top of the spectrograph) and for L1C row 50 in northern hemisphere scans (bottom of the slit). Use of a single PSF for the entire slit in algorithms to retrieve temperature from LBH band shapes can introduce a latitude dependent bias to higher temperatures.

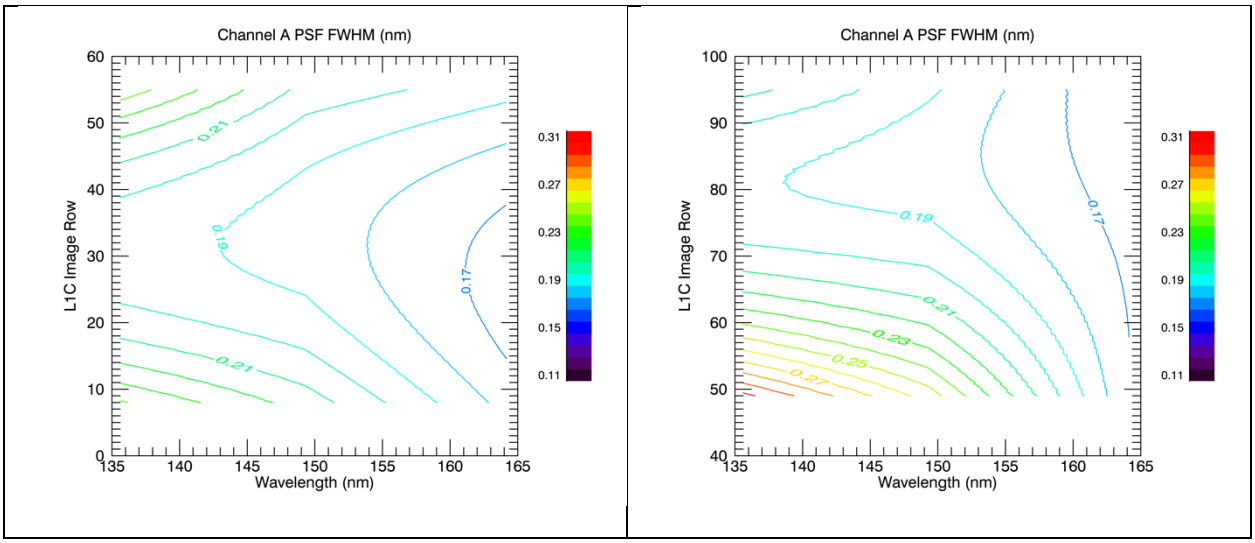

Figure 3-10 Contour plots of FWHM for GOLD's spectral point spread function

3.1.12 Errors in the L1C Wavelength Scale

A single wavelength scale is assigned to all spectra in an L1C image cube. It is calculated by coadding all the spectra in the cube to form a total spectrum and fitting the positions of the atomic lines of the OI 135.6 nm doublet and the NI 149.3 nm triplet to a linear function. (Early in the mission, an OI 164.13 nm was also used in the fit but is not now available since GYM actuations have moved it out of the spectrograph pass band after August 10, 2020).

Figure 3-11 compares the average wavelength scale solution to the solutions for the individual rows in an L1C data cube. The left panels are plots of the differences between the wavelength of pixel 0 (800-element (0 – 799)) in the scale fit to each row and the wavelength of pixel 0 in the scale fit to the spectrum of all spatial pixels. The top includes rows 8 – 55 (southern hemisphere L1C file) and the bottom includes rows 40 – 95 (northern hemisphere L1C file). These indicate that the starting wavelength in each row typically varies by less that 0.5 pixels (0.02 nm) over most of the L1C image cube. The right panels are plots of the differences between the total length of the wavelength range (typically 32 nm) for scale fit to each row and the scale fit to all spatial pixels. These results are valid for wavelength scales derived by fitting 3 wavelengths (135.6, 143.9 and 164.13) or by fitting only the first two wavelengths. These results indicate that the single solution is accurate to better than ±1 pixel or better. Currently, researchers requiring better accuracy should use their own fitting routines.

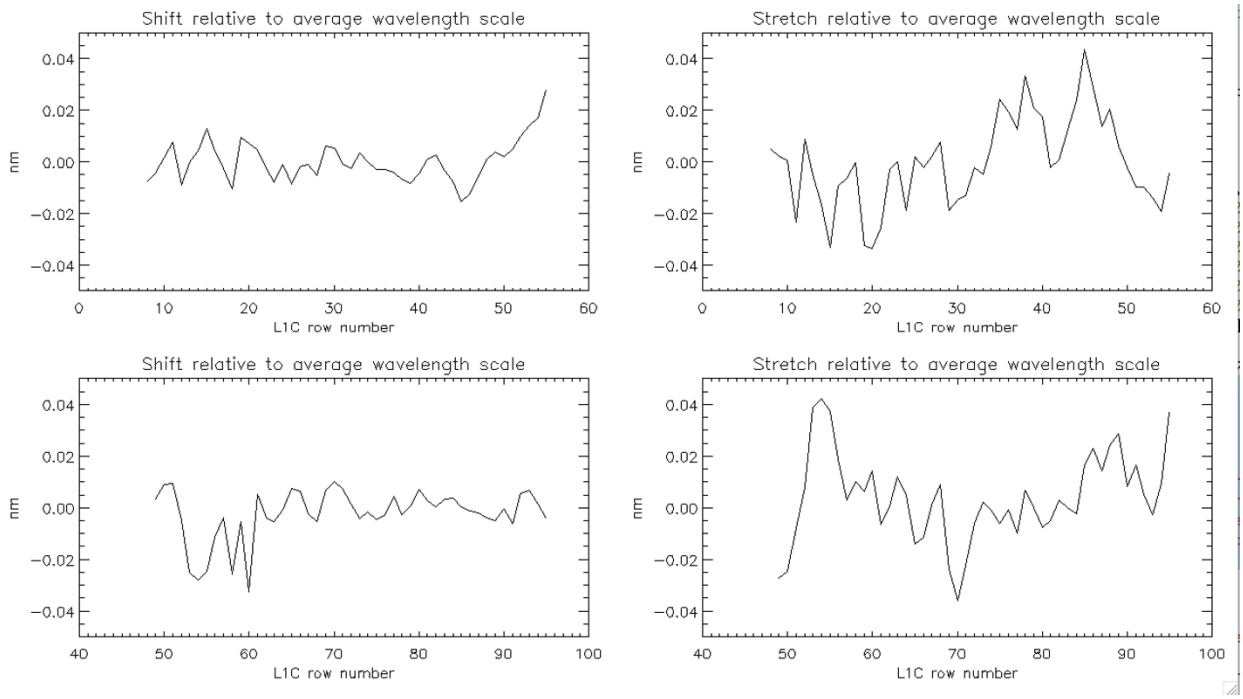

Figure 3-11 Wavelength scale shift-stretch for individual L1C image cube rows relative a wavelength scale for the entire

3.1.13 No Moon Flag

The presence of the Moon in the field of view is currently not being flagged during processing. This could affect the Limb and Occultation measurements. This issue will be addressed in future releases.

3.1.14 No Xenon Emission Flag

The SES-14 spacecraft that hosts the GOLD instrument uses ion propulsion for spacecraft station-keeping maneuvers. Its thrusters use xenon gas as a propellent, and it has been found that the GOLD instrument sees a xenon emission line at 146.96nm during these maneuvers. A quality flag that indicates the presence of this spectral feature will be added in a future release.

3.1.15 Noise due to High Particle Background

Particles from the radiation belt(s) produce counts in the detectors of GOLD and can appear as bright, noisy pixels when the particle background levels are high. Periods of high particle background are flagged in the L1C DAY, LIM, and NI1 data through the use of a global attribute named “High Background”. Some examples of such noisy data are shown in Figure 3-12 and Figure 3-13.

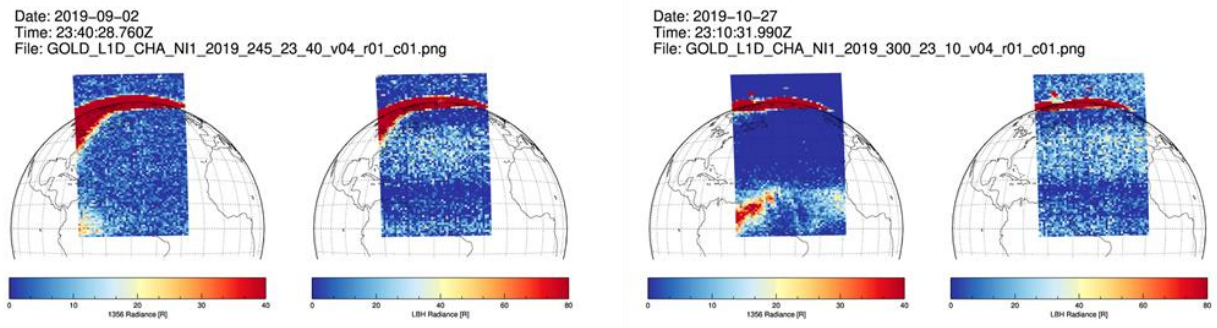

Figure 3-12 Examples of bright noisy pixels in night time images due to high particle background

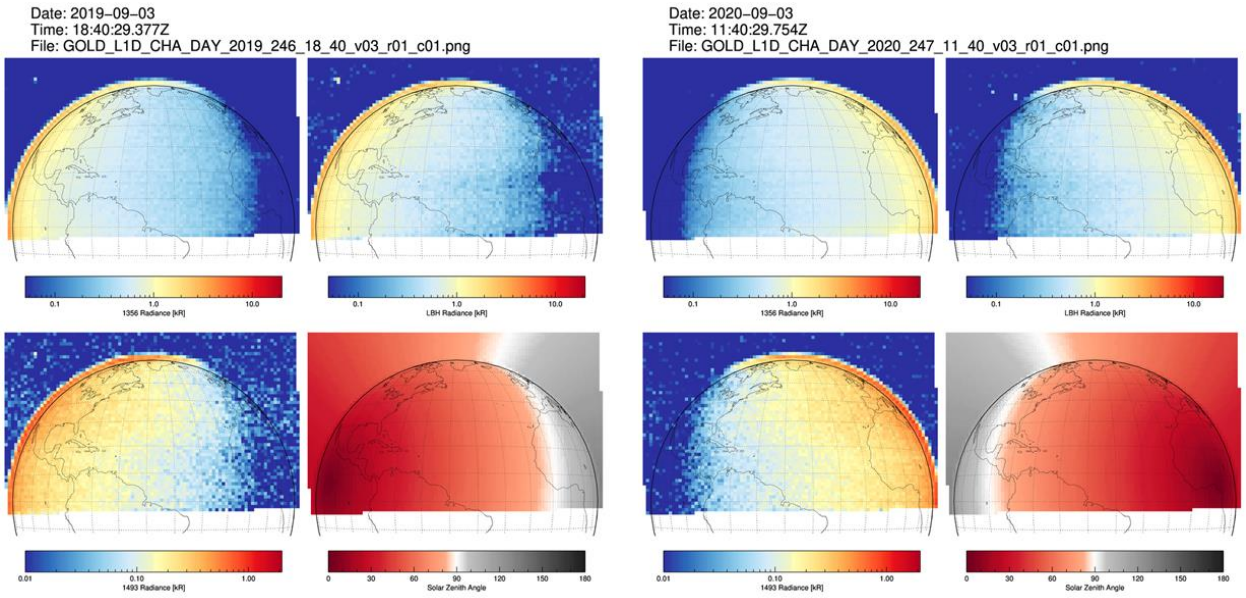

Figure 3-13 Noisy pixels in day time images due to high particle background; more prominent in the LBH emissions which have lower B(R) per pixel, but similar background per pixel

3.1.16 Field emission type events

Some anomalous events occur on the GOLD Channel A detector in both DAY and NI1 observations at LBH wavelengths. These events are most apparent in the night (NI1) images as seen in Figure 3-14. They appear at mid latitudes between 15^{o} to 60^{o}. These may be due to field emission events within the detector housing. Their position on the detector corresponds to

midlatitudes (vertically) and within the wavelength range of the LBH band emissions (horizontally). Such events are not flagged in the released data.

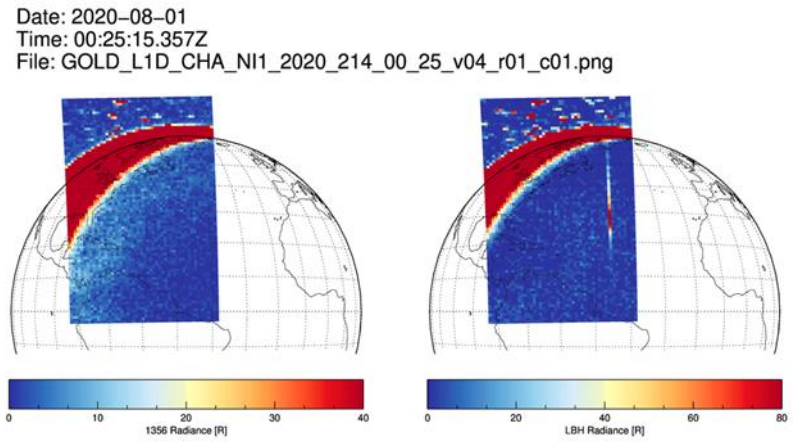

Figure 3-14 Example of field emission type events

3.1.17 Effect of stars on the brightness

When a star comes into the limb of the Earth, it appears as a bright spot in the image as shown in Figure 3-15. The starlight can scatter to pixels along the slit and can result in a bright vertical band in the image. These events are not flagged in the released data.

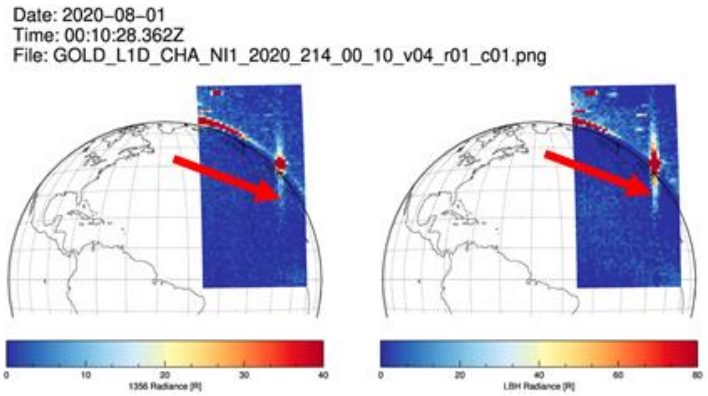

Figure 3-15 Scattering of starlight to pixels along the instrument slit

3.1.18 Horizontal artifacts in Channel B NI1 scans

On some days, the current pulse height filtering and flat-field correction may introduce horizontal artifacts in the L1C CHB NI1 images. These artifacts are due to the high voltage being too low during the flat-field measurement. The artifacts appear as depleted (left panel, Figure 3-16) or enhanced (right panel, Figure 3-16) horizontal stripes in the OI 135.6 nm emission observations. These are not flagged in the released data.

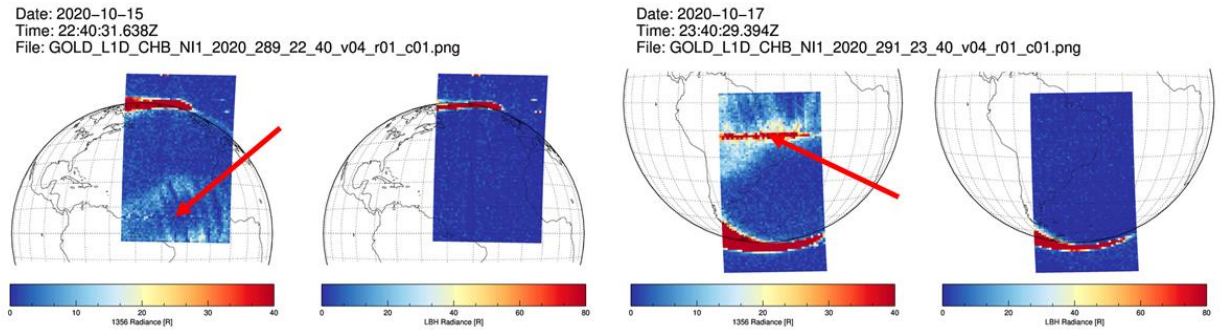

Figure 3-16 Horizontal stripes in Channel B NI1 scans due to limitations in the pulse height filtering and flat-field correction.

3.1.19 Artifacts in first DAY scan after an instrument safe-hold (or error recovery)

In rare cases, the GOLD instrument enters safe mode (e.g., when the bright object sensor is triggered). When the instrument is brought out of safe mode, the first DAY image scan may exhibit an artifact like in Figure 3-17, where a blue strip corresponding to zero radiance is seen on the right side of the image. This artifact occurs because the detector high voltage is not fully ramped up when the scan starts. The high voltage ramps up rather quickly, and most of the scan is valid. However, the part of the image near the artifact should be disregarded. This artifact may also occur in the first DAY scan after observations are interrupted to perform an error detection and correction (EDAC) error recovery.

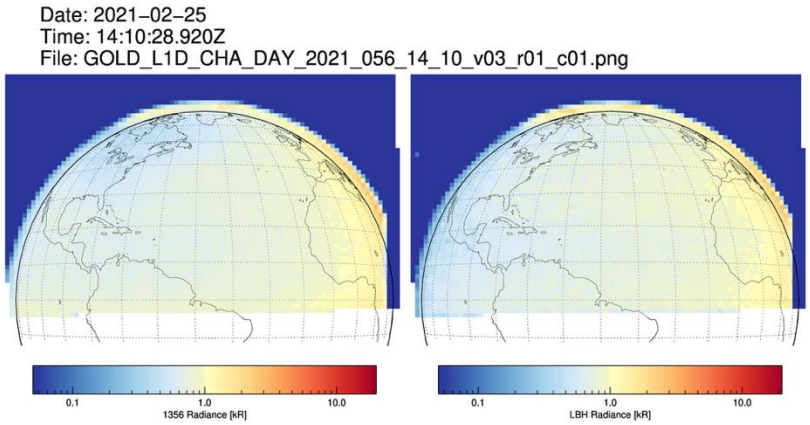

Figure 3-17 Artifact in DAY image after instrument safe-hold

3.1.20 Incorrect metadata values in Level 1C occultation files

The following global attributes present in the Level 1C occultation data products are populated with incorrect values: SC_Alt, SC_Pos, SC_Z_Dir, SC_Nadir_lat, SC_Nadir_lon, SC_Yaw. In order to correct values for these entries, divide the reported value by 2940.

3.1.21 Incorrect Values for Radiance Systematic Uncertainty in the L1C Files

The values for the radiance_systematic_unc underreport the magnitude of the uncertainty in this variable. To first order, a reasonable range of estimate is 0.15*radiance < radiance_systematic_unc < 0.2*radiance, i.e., the relative uncertainty is ~ 15 – 20 %.

3.1.22 Vertical depletion artifacts in Level 1 NI1 data

Occasionally, Level 1 NI1 data exhibit vertical depletion artifacts like the ones seen in Figure 3-18. These artifacts are caused by the time-dependent background subtraction when the signal from a star is located in the area of the detector that is used to determine the background level.

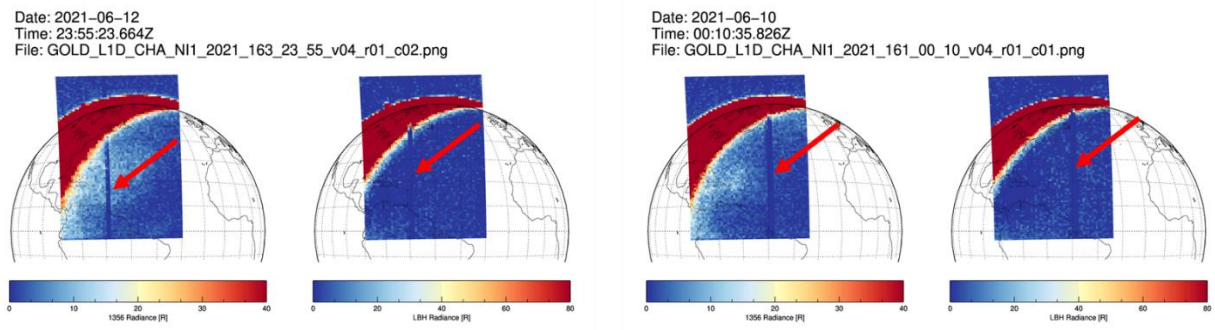

Figure 3-18 Vertical depletion artifacts in L1 NI1 data

3.2 Level 2

All GOLD Level 2 files contain arrays for three separate components of the total error in retrieved geophysical parameters – random, systematic and model errors. In general, the error characterization for the Level 2 data products in this release is preliminary. Specifics for each data product are described in the sections that follow.

Each Level 2 data product file contains a list of data quality indices (DQI) specific to that data product. These DQI are defined at both the file and individual pixel level and are described in detail in the ***GOLD Science Data Product Guide*** (available on the GOLD website)**.** That document also contains a description of each Level 2 data product, including a summary of the algorithm theoretical basis and a complete description of the contents of each Level 2 daily NetCDF file.

3.2.1 Issues with O2DEN data

3.2.1.1 Preliminary error analysis

A comprehensive error analysis and retrieval characterization for the O2DEN product is in progress but has not yet been implemented in this release. Currently only the random error array

is populated in the O2DEN files. These errors should be considered preliminary until the detailed error analysis is implemented.

3.2.1.2 Valid altitude range in retrieved O_2 profile

The O2DEN data product – density profile of molecular oxygen (O_2) retrieved from stellar occultation (OCC) measurements – is retrieved on a fixed geometric altitude grid. However, the altitude range of the retrieved profile varies for each event (altitudes above and below the valid retrieval range for each event are populated by fill values). This is because the algorithm truncates the input measured atmospheric slant path transmission profiles to a fixed transmission range before input to the optimal estimation routine. A given transmission value will correspond to different tangent altitude levels as the absolute O_2 number density varies with geophysical conditions.

Pending a more complete retrieval characterization analysis to accompany the error analysis in a future release, a preliminary sensitivity study has been performed to characterize the degree of *a priori* bias in the O_2 retrievals. Figure 3-19 summarizes the results of this analysis. It shows the relative difference, in %, between the retrieved O_2 profile and the *a priori* profile for a random sample of ~500 occultations over 60 days. Difference profiles for the individual occultation events are shown in the left panel and daily averages are on the right. These plots clearly illustrate the behavior described above, with the retrieved O_2 converging to the *a priori* at both high and low altitudes. Based on this analysis it is recommended that users assign the highest confidence to the altitude region between 130 and 190 km, which contains the most independent information on the absolute O_2 density profile. This range is denoted by the dashed horizontal lines in Figure 3-19. Currently the error bars and DQI reported in the O2DEN data files do not capture this data quality metric.

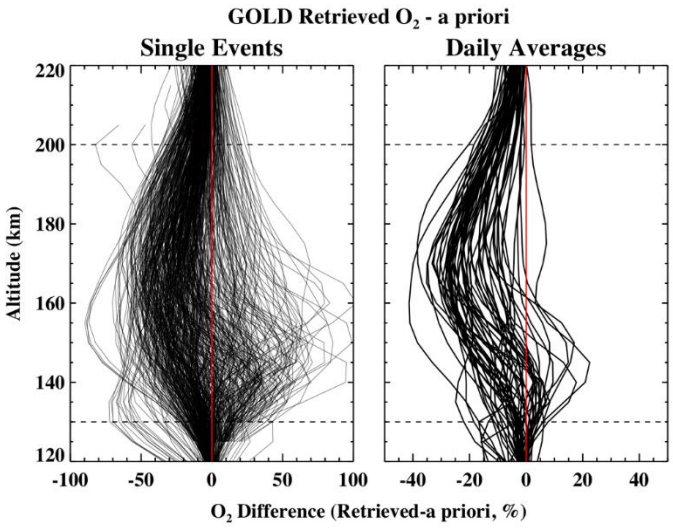

Figure 3-19 Variance between retrieved O2 profile and retrieval a priori.

3.2.1.3 Possible residual background bias in dayside O2DEN data

GOLD performs occultation measurements on both limbs at all times during the day. Therefore, on average approximately half of the O2DEN retrievals are obtained on the sunlit limb. Under these conditions it is particularly important that the atmospheric airglow background be accurately removed from the data in the L1C processing. Small residual errors in the background removal can in principal cause increased noise or systematic bias in the O_2 profile, particularly for events using the dimmer stars in the GOLD target star list. Both dayside and nightside data (Channel A only) are contained in this release. While users are not discouraged from using the dayside retrievals, for a more conservative screening of the data users can easily identify these events using the "dayside" flag in the event level DQI array, or by simply paying attention to the measurement solar zenith angle (an approximate flag for dayside events is SZA < 100 degrees).

3.2.1.4 Data gaps

There is a gap of approximately one month in the O2DEN data set, from December 17, 2018 to January 13, 2019. During this time period there was a glitch in the GOLD operational planning that caused errors in the instrument pointing and timing, resulting in missed occultations. This data is not recoverable since no underlying L1C data were obtained.

3.2.1.5 Timing errors

The onboard clock is used to assign UT time stamps to individual measurements in the GOLD Level 1A processing. For the occultation (OCC) data processing these time stamps are then used to generate the geolocation information (primarily tangent point latitude, longitude, and altitude) for the target star as it passes through the GOLD slit. The onboard clock time drifts relative to true time, with errors that depend on temperature and can be of either sign. Generally, the clock drift accumulates slowly and systematically but the drift rate can accelerate during times of increased daily temperature variations such as during eclipse season. The clock offset is monitored and when it gets large enough an offset is applied to zero it out. The magnitude of the timing error has reached 3 sec twice during the GOLD mission but is generally less than 2 seconds.

The primary impact of the time stamp error is to cause an error in the slant path tangent altitude grid assigned to the L1C OCC data. This altitude offset is essentially constant for a given event and maps directly into the normalized atmospheric transmission profiles generated from the L1C irradiance data and used as input to the L2 O2DEN algorithm.

The magnitude of the tangent altitude error can be estimated from the known clock drift using the following equation:

$$\Delta Z = (-1)\Delta t \left(3\frac{km}{s}\right)\cos(\varphi)\, sign(\lambda) \qquad (Eq.1)$$

where ΔZ is the error in km, Δt is the clock drift in seconds, 3 km/s represents the altitude rate of change across the slit for a star rising or setting at the equator, φ is the occultation latitude, and λ is the occultation longitude (longitude is a proxy for distinguishing star rise events – East limb/positive longitude – from star sets – West limb/negative longitude). ΔZ is generally within 5-7 km for most of the GOLD data, but has occasionally reached as high as 10 km.

It is worth emphasizing again that the error calculated from Eq. 1 applies to the L1C slant path tangent altitudes. This propagates through the retrieval algorithm, resulting in errors in the geometric altitude grid assigned to the retrieved O_2 density profile. Due to the limb inversion process the final altitude errors in the O_2 profile are not identical to what is calculated from Eq. 1.

Nevertheless, as a first order correction to the current V03 data set users can apply the correction calculated from Eq. 1 directly to the O_2 profiles archived in the Level 2 data files. The clock drift as a function of UTC time is available as a CSV file from the GOLD website on the "Tools" page: https://gold.cs.ucf.edu/data/tools. The file has the average clock drift (in msec) over 15-minute increments. To calculate the altitude correction, you would find the UTC time in the file that is closest to the time of the occultation and use the corresponding clock drift in the equation above.

A fix for the clock offset error is planned for a future release. This will result in accurate UTC times, and hence geolocated altitudes, for all GOLD occultation data. At that point the O2DEN data will be reprocessed, and a new version released.

3.2.2 Issues with TLIMB data

The primary issues with TLIMB data are degraded performance at large solar zenith angles and occasional failure of the algorithm to converge to a physical solution.

3.2.2.1 Preliminary error analysis

A comprehensive error analysis and retrieval characterization for the TLIMB product is in progress but has not yet been implemented in this data release. Currently only the random error array is populated with non-fill values in the Level 2 files. These errors should be considered preliminary until a more detailed error analysis is performed.

3.2.2.2 Stars in the field of view

It is common for stars to be observed within the field-of-view of the detector during limb scans. An example showing multiple stars within the field-of-view can be seen in Figure 3-20. When a star appears in the field-of-view it can alter the shape of the N_2 LBH limb profile producing systematic biases in retrieved exospheric temperatures. Therefore, the TLIMB algorithm code implements a star detection algorithm that utilizes the difference between stellar and airglow spectra. When a star is detected in the field-of-view the TLIMB algorithm is not run and the

corresponding DQI is set to a non-zero value. Note that the star detection algorithm is not 100% reliable, thus false positive and negative detections may occur. Users are advised to independently review the Level 1C data for stars in the field-of-view when working with the TLIMB data

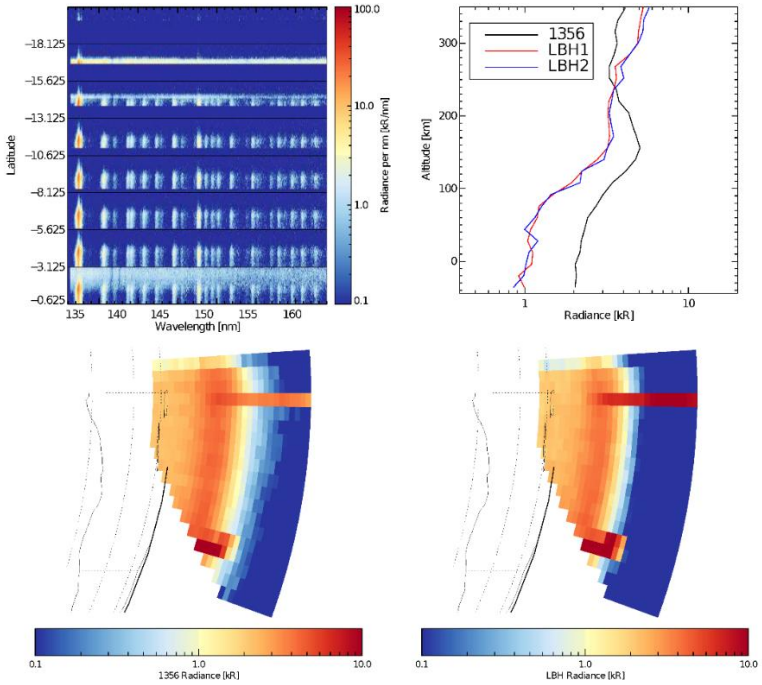

Figure 3-20 Level 1D plot showing observation of multiple stars in the field-of-view during a limb scan.

3.2.2.3 Latitude constraints

The signal-to-noise ratio at the edge of the detector (on the equatorward, north end of the slit) is typically low during southern hemisphere scans, which can produce systematic biases in retrieved temperatures. Therefore, the TLIMB algorithm is not run (TLIMB is set to fill value and DQI set to non-zero value) when the latitude of southern hemisphere limb scan data is greater than 2.5 degrees. Note that northern hemisphere scans may also be affected by low signal-to-noise at the edge of the detector (south end of the slit), though no latitude constraint is currently imposed for northern scans. Users are advised to use caution when working with TLIMB data derived from the edges of the detector.

3.2.2.4 Tangent altitude constraints

The TLIMB algorithm is only run if the tangent altitudes span the range from 250 km (or higher) to 160 km (or lower) and there are no NaNs in the corresponding Level 1C LIM brightnesses or uncertainties. If this condition is not met, the TLIMB value is set to a fill value and the corresponding DQI is set to a non-zero value.

3.2.2.5 Degraded performance at large solar zenith angle

When the solar zenith angle is between 60 and 90 degrees the TLIMB algorithm is run but a corresponding DQI is set to a non-zero value indicating the potential for degraded algorithm performance. The algorithm is not run when the solar zenith angle is greater than 90 degrees. Degradation at high solar zenith angles primarily affects the TLIMB data on the East limb as viewed from GOLD (positive longitudes in the Level 2 file). Users should apply extra caution when working with TLIMB data products when algorithm performance is degraded, particularly the data on the East limb at solar zenith angles greater than 70 degrees.

3.2.2.6 Algorithm failure

Occasionally the TLIMB algorithm will fail to converge when fitting an observed N_2 LBH limb profile. If the algorithm fails to retrieve an exospheric temperature the TLIMB value is set to a fill value and the corresponding DQI is set to a non-zero value.

3.2.2.7 Data gaps

There is a gap of one day in the TLIMB data for October 9, 2018, when the TLIMB retrievals are anomalously high. This could be related to high particle background levels on that day, although this is inconclusive at this time.

3.2.3 Issues with TDISK data (updated 8/5/2022)

3.2.3.1 Preliminary error analysis

A comprehensive error analysis and retrieval characterization for the TDISK product is in progress but has not yet been implemented in this data release. Currently only the random error array is populated with non-fill values in the Level 2 files. These errors should be considered preliminary until a more detailed error analysis is performed.

3.2.3.2 Algorithm limits

The TDISK algorithm code is not run when the solar zenith angle exceeds 80 degrees, or the emission angle exceeds 75 degrees.

3.2.3.3 Algorithm failure

Occasionally the TDISK algorithm will fail to converge when fitting an observed spectrum. If the algorithm fails to retrieve an effective neutral temperature the TDISK value is set to a fill value and the corresponding DQI is set to a non-zero value.

3.2.3.4 Effective altitude.

As with any satellite nadir (disk) viewing measurement, the GOLD DAY disk observations sample all altitudes along a given line of sight, from the top of the atmosphere to below the peak

of the emitting layer. The observed temperatures are weighted by the peak volume emission rate at altitudes where there is a significant temperature gradient (~150-200 km). Since the GOLD disk observations represent a column integration of the weighting function (i.e. there is no altitude information), the effective height of the derived TDISK temperature product, which varies with viewing conditions (solar zenith angle and, to a lesser extent, emission angle) must be determined with the aid of forward modeling. This work has not yet been completed as of present release and thus we report a default value of NaN for the effective altitude. We note for clarity that previous data versions recorded a value of 150 km for the TDISK effective altitude. This reference altitude level is used to geolocate pixels for the GOLD DAY disk data, however the reported TDISK values are not intended to be representative of this altitude.

3.2.3.5 Sources of contamination

One potential source of contamination that may produce artifacts in the TDISK retrieved temperatures is energetic particle flux in the polar regions. At present, there is no auroral boundary detection algorithm implemented in the Level 2 operational pipeline, and users are therefore advised to use caution when working with TDISK data when the geomagnetic latitude exceeds 60 degrees.

3.2.3.6 Discontinuities around GYM actuations

As discussed in Section 3.1.1, an operation called a GYM actuation is occasionally implemented to mitigate the effects due to detector burn-in (the GYM actuation dates are listed in Table 2-1). The TDISK data can exhibit discontinuities before and after the GYM actuation operations, as illustrated in Figure 3-21. This artifact primarily affects TDISK around the first, fourth and fifth GYM actuations (April 26 2019, August 11 2020, and February 8 2021). TDISK values show an immediate drop after these dates, with a recovery time ranging from ~5 to 15 days. Caution is advised when using the TDISK data for times near any GYM actuation operation.

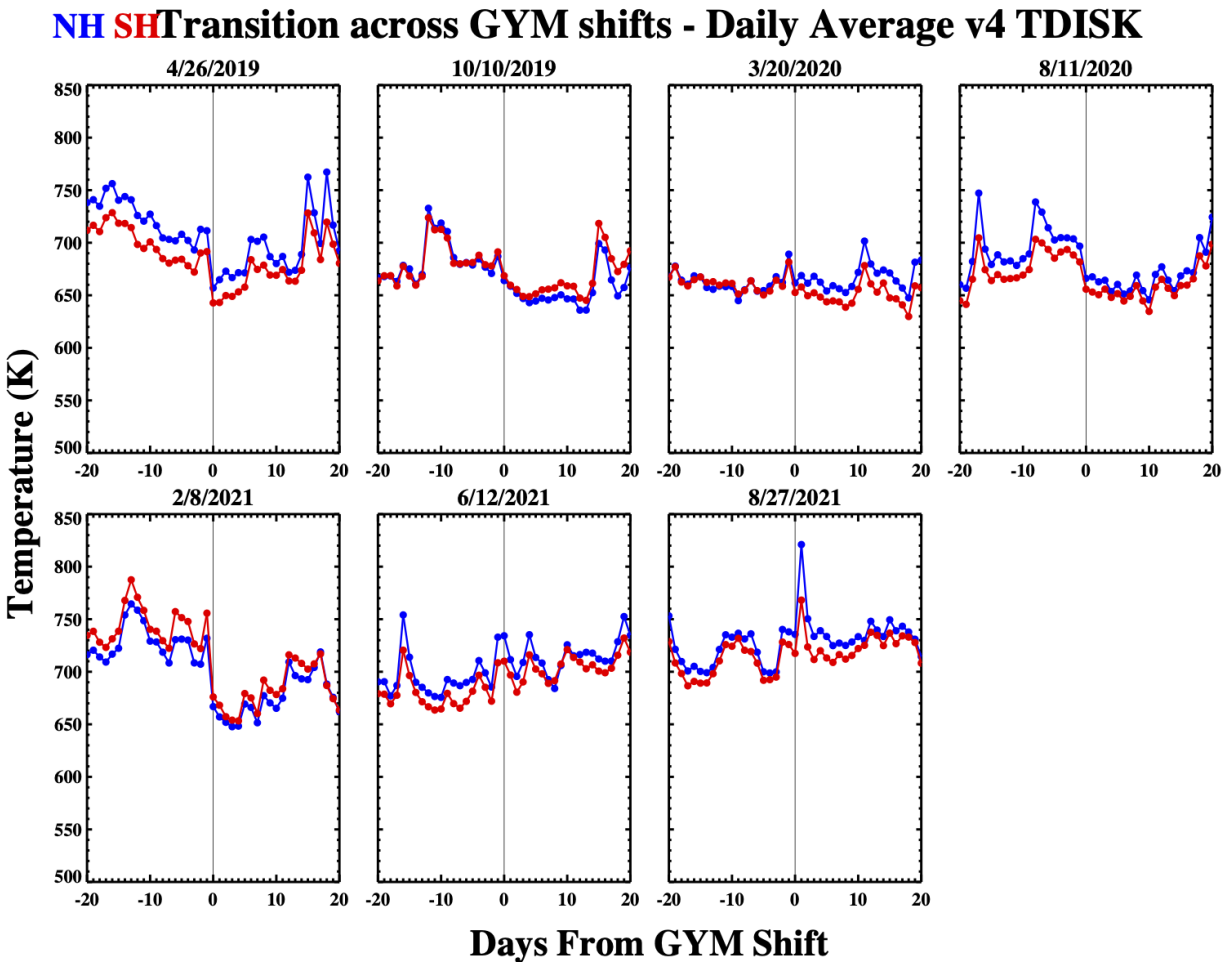

Figure 3-21 Daily average TDISK v04 data before and after the Channel A GYM shift operations to date. Northern/Southern hemisphere (NH/SH) are plotted in blue and red, respectively. In each panel the vertical solid line is the date of the GYM operation.

3.2.4 Issues with ON2 data

The primary issues affecting ON2 data quality are related to the degradation of measured O I 135.6 nm emission brightness due to detector burn in. The impact of these artifacts in the ON2 data can vary with season and time of day, depending on the state of the instrument and the effectiveness of corrections used to mitigate detector burn-in. End users are advised to exercise caution when interpreting ON2 values during times of increased L1C data artifacts described below. ON2 is most useful as a measure of relative changes in the atmosphere, and it is suggested that users apply analysis techniques that tend to minimize effects due to instrument artifacts, e.g., taking deviations relative to a daily mean, or differencing the same times during consecutive days. Direct comparison of ON2 values over large time differences (more than several days) require particular care.

3.2.4.1 Preliminary error analysis

A comprehensive review of errors associated with ON2 is in progress. Uncertainty values in ON2 files should be considered preliminary.

3.2.4.2 Algorithm limits

The O/N_2 algorithm is not run when the solar zenith angle is greater than 80 degrees and the emission angle is greater than 75 degrees. Also note that DQI flags are not set bitwise.

3.2.4.3 Contamination of ON2

The O/N_2 algorithm is only valid when the source of O I 135.6 nm and N_2 LBH emission is photoelectrons generated by solar EUV flux. Other sources of these emissions are considered contaminants and will result in erroneous derived O/N_2 values. The main sources of the contaminant emissions for the O/N_2 algorithm are energetic particle precipitation in the polar regions (affecting both 135.6 nm and LBH) and radiative recombination of O^+ in the equatorial ionization anomalies (affecting only 135.6 nm). At present, there is no auroral boundary detection algorithm implemented in the Level 2 operational pipeline, therefore users are advised to use caution when working with ON2 data where the geomagnetic latitude exceeds 60 degrees. Similarly, users are advised to use caution when working with ON2 data during geomagnetically active periods that may produce enhanced radiative recombination emission in the equatorial ionization anomalies.

3.2.4.4 Hemispheric bias

The residual gradient in instrument sensitivity described in Section 3.1.2 causes small biases in the measured radiances in the along-slit direction (essentially North-South). This artifact is greatest at short wavelengths, and hence affects the oxygen 135.6 nm band brightness more than LBH. These radiance biases produce similar biases in the derived ON2 values (even though ON2 is derived from the ratio of 135.6 nm and LBH band intensities, the wavelength dependence of residual, along-slit sensitivity biases means that the effect does not cancel). The largest manifestation of this effect is seen in ON2 derived near the equator, since these pixels are sampled by opposite ends of the slit in the Northern hemisphere (NH) and Southern hemisphere (SH) scans. The net result is an offset of approximately 5-10% on average in ON2 (SH higher than NH) at the equator. This will show up as a banding artifact along the equator in a full global ON2 image created from consecutive NH and SH scans.

3.2.4.5 Discontinuities around GYM actuations

As discussed in Section 3.1.1, an operation called a GYM actuation is occasionally implemented to mitigate the effects due to detector burn-in (the GYM actuation dates are listed in Table 2-1). The ON2 data sometimes exhibits discontinuities immediately before and after this operation, driven primarily by abrupt changes in the 135.6 nm radiance, as illustrated in Figure 3-22. This artifact is evident in the ON2 data to some extent at all GYM actuations. ON2 values

immediately before and after these operations show a difference in overall magnitude as well as distinctly different local time dependence throughout the day (not shown in Figure 3-22). Caution is advised when using the ON2 data for times near any GYM actuation operation.

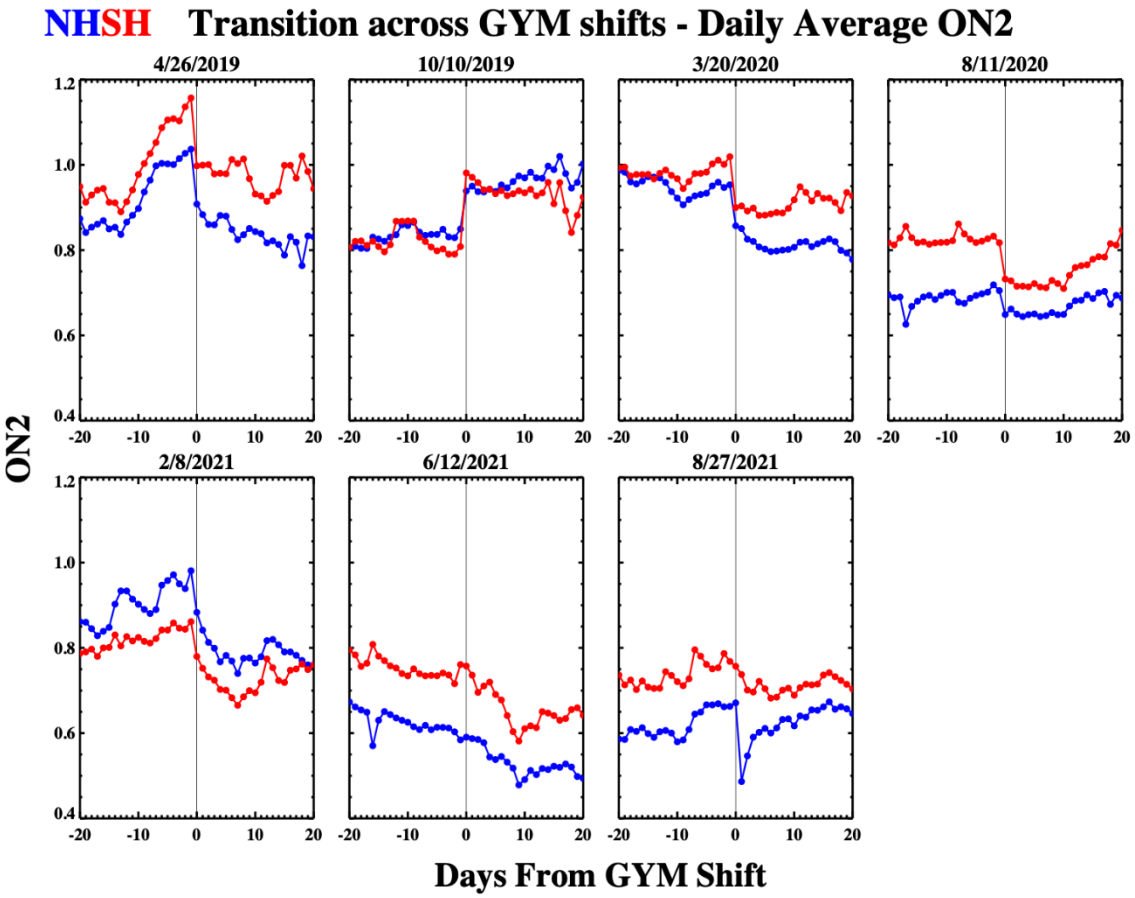

Figure 3-22 Daily average ON2 data before and after the Channel A GYM shift operations to date. Northern/Southern hemisphere (NH/SH) are plotted in blue and red, respectively. In each panel the vertical solid line is the date of the GYM operation.

3.2.4.6 Flat Field correction artifacts

The flatfield correction has some limitations that affect ON2. As discussed in Section 3.1.5 the flatfield correction can sometimes under- or over-correct data depending on time of day and season. Errors in the flatfield correction are largest in the 135.6 nm band during periods when a significant correction is needed, such as the weeks preceding a GYM actuation. These errors can appear as biases and/or enhanced scatter in the ON2 data. See Figure 3-23, where the flatfield correction errors result in horizontal bands of depleted or enhanced O/N_2 just below the equator.

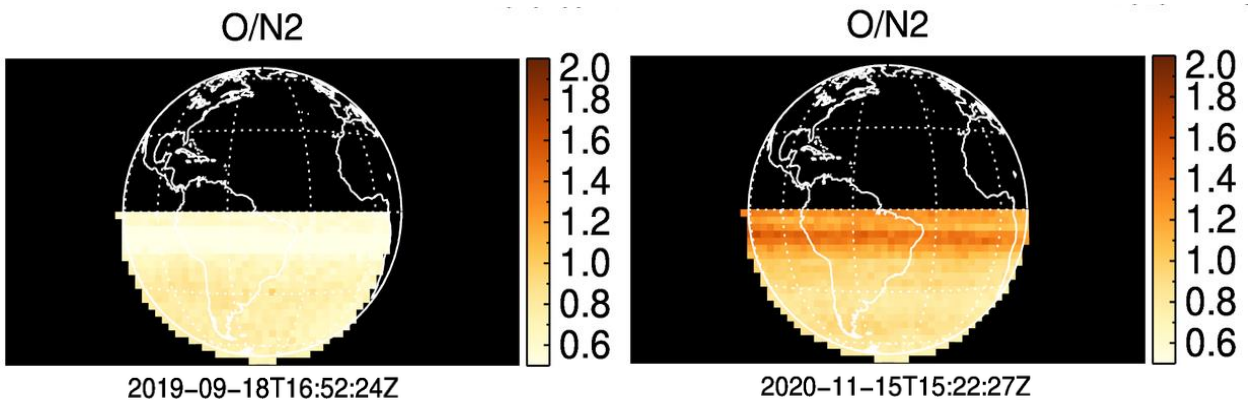

Figure 3-23 Examples of the impact of flat field correction errors on the ON2 data product. The errors result in horizontal bands of depleted or enhanced O/N_2

3.2.4.7 Effects due to high particle background

Conditions of high particle backgrounds at the spacecraft can sometimes cause increased scatter in the ON2 retrievals. Two such periods of note are September 26 – October 5 and October 24 – November 1, 2020. Users are advised to use extra caution when working with ON2 data products during periods of enhanced particle background.

3.2.5 Issues with QEUV data

Like ON2, the QEUV parameter is derived from measurements of the O I 135.6 nm and N_2 LBH emission radiances. The primary issues affecting QEUV data quality are sensitivity to instrument degradation, flat field corrections, and other effects, particularly with the 135.6 nm intensities.

3.2.5.1 Preliminary error analysis

A comprehensive review of errors associated with QEUV is in progress. Uncertainty values in QEUV files should be considered preliminary.

3.2.5.2 Algorithm limits

The QEUV values are not derived where the solar zenith angle is greater than 80 degrees, The QEUV values are not derived where the solar zenith angle is greater than 80 degrees, emission angle is greater than 75 degrees and the time of the DAY disk scan is between 10- and 20-hours UTC. Also note that DQI flags are not set bitwise.

3.2.5.3 Contamination of QEUV

As with ON2 the QEUV algorithm is only valid when the source of O I 135.6 nm and N_2 LBH emission is photoelectrons generated by solar EUV flux. Other sources of these emissions are considered contaminants and will result in erroneous derived QEUV values. The main source of the contaminant emissions for the QEUV algorithm is radiative recombination of O^+ in the equatorial ionization anomalies (affecting only 135.6 nm). Users are advised to use caution when

working with QEUV data during geomagnetically active periods that may produce enhanced radiative recombination emission near the equatorial ionization anomalies.

3.2.5.4 Hemispheric bias

There is a small bias between the QEUV values derived from near-coincident Northern Hemisphere (NH) and Southern Hemisphere (SH) scans, with SH values are higher than NH. This difference seems to have a seasonal component, ranging from a maximum of ~10% in the NH summer to near zero in NH winter. Part of this issue is related to the gradient in instrument sensitivity along the slit described in Section 3.1.2. As with the ON2 data product, the North/South bias in the measured 135.6 nm radiances propagates into the QEUV retrieval. The seasonal component of this bias in QEUV seems to another possible source of error that is under investigation.

3.2.5.5 Discontinuities around GYM actuations

As discussed in Section 3.1.1, an operation called a GYM actuation is occasionally implemented to mitigate the effects due to detector burn-in (the GYM actuation dates are listed in Table 2-1). The QEUV data exhibits discontinuities immediately before and after the GYM actuation operations, driven primarily by abrupt changes in the 135.6 nm radiance. This is illustrated in Figure 3-24. The artifact is most significant in QEUV at the first, fourth and fifth GYM actuations, and to a lesser extent at the others. QEUV values immediately before and after these operations show a jump in magnitude. Caution is advised when using the QEUV data for times near any GYM actuation operation.

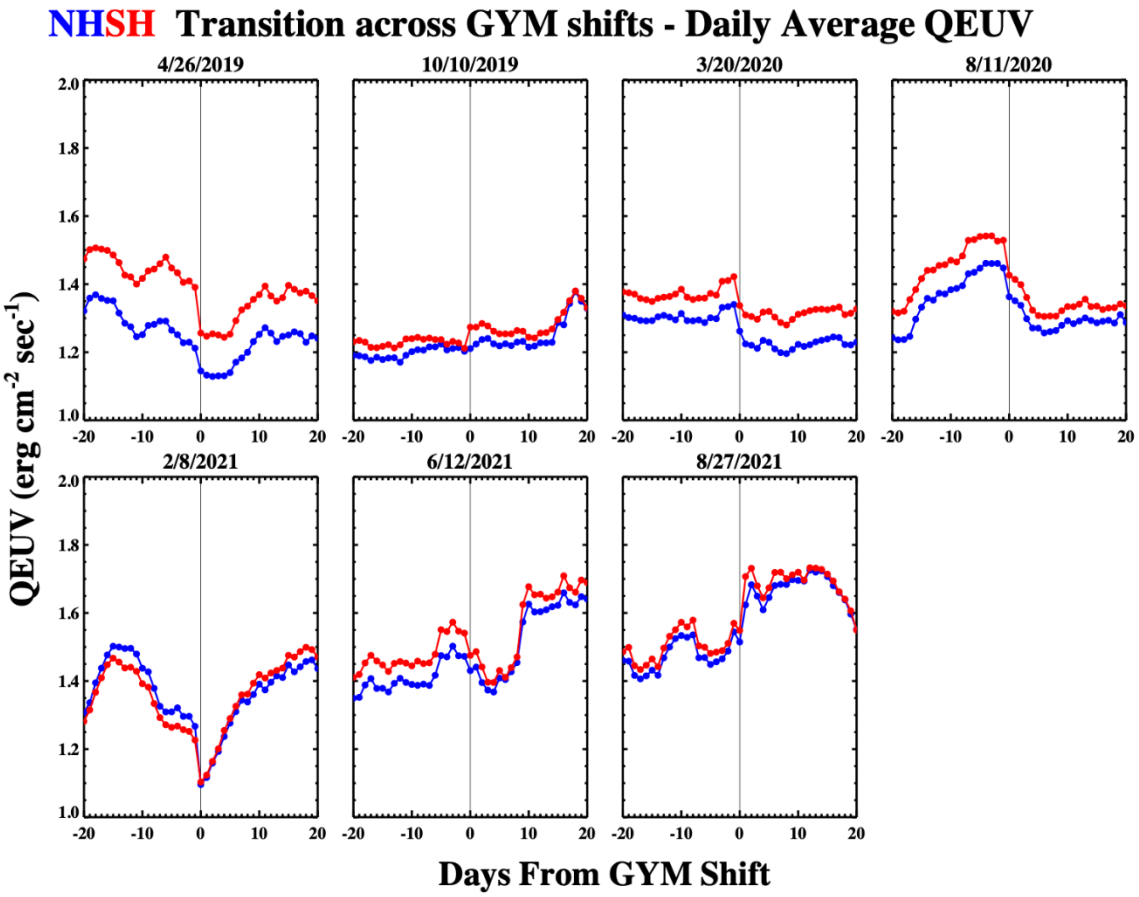

Figure 3-24 Daily average QEUV data before and after the Channel A GYM shift operations to date. Northern/Southern hemisphere (NH/SH) are plotted in blue and red, respectively. In each panel the vertical solid line is the date of the GYM operation.

3.2.5.6 Flat Field correction artifacts

The flatfield correction has some limitations that affect QEUV. As discussed in Section 3.1.5 the flatfield correction can sometimes under- or over-correct data depending on time of day and season. Errors in the flatfield correction are largest in the 135.6 nm band during periods when a significant correction is needed, such as the weeks preceding a GYM actuation. These errors can result in biases and/or enhanced scatter in the QEUV data during these periods.

3.2.6 Issues with NMAX data

3.2.6.1 Model uncertainty

Because the current NMAX algorithm neglects two sources of 135.6 nm photons (ion-ion mutual neutralization: $O^+ + O^- \rightarrow O + O + h\nu$ and resonant scattering of 135.6 nm photons by atomic oxygen), it tends to overestimate the value of NMAX. We estimate that the model error due to the omission of these two sources is approximately 15% (that is +15% and −0%) depending on

several variables mainly having to do with atmospheric composition and variability in the electron density profile shape.

3.2.6.2 Flat Field correction artifacts

On some days, the current pulse height filtering and flat-field correction may introduce horizontal artifacts in the L1C CHB NI1 images (see section 3.1.18). These artifacts will also propagate through to the L2 CHB NMAX data, as seen in the example in Figure 3-25 below. These are not flagged in the data.

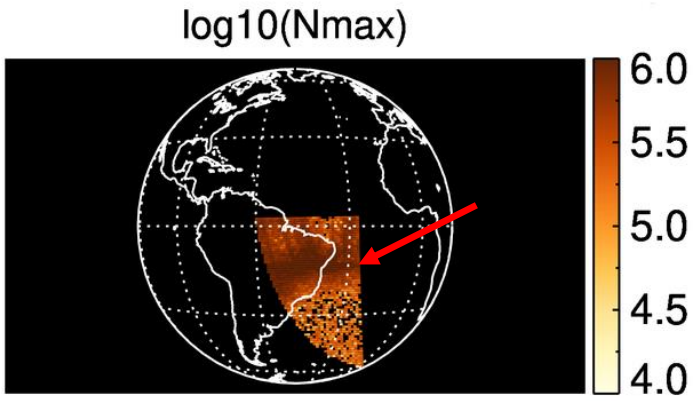

Figure 3-25 Horizontal stripe in the CHB NMAX data due to issues in the flat-field correction of the L1C NI1 data.

3.2.6.3 Vertical Depletion Artifacts

Occasionally, NMAX data exhibit vertical depletion artifacts like the ones seen in Figure 3-26. These artifacts are also evident in L1C NI1 data (Section 3.1.22) and are caused by the time-dependent background subtraction when the signal from a star is located in the area of the detector that is used to determine the background level.

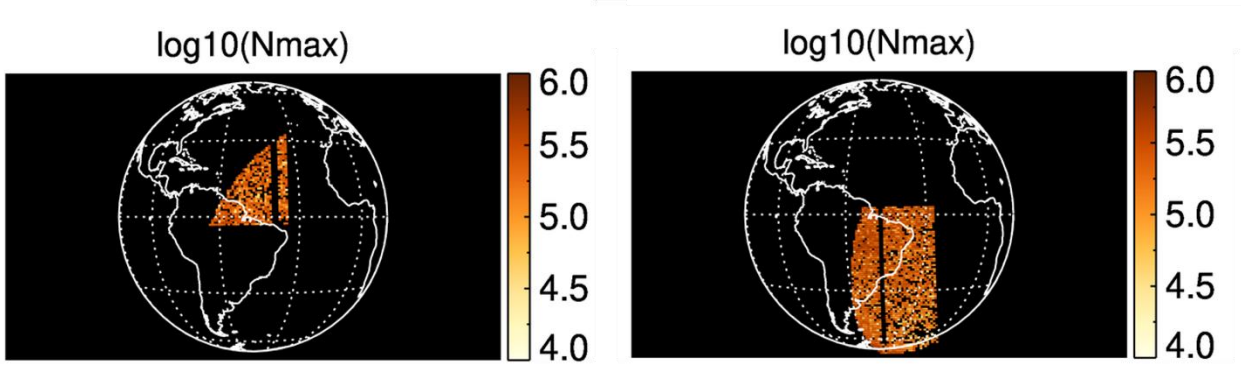

Figure 3-26 Vertical depletion artifacts in NMAX data

3.2.6.4 Data Gaps

There is a large data gap in the Channel B data between Dec 15, 2018 and Mar 15, 2019 due to a detector burn in problem, which renders the Channel B NI1 data taken during that time useless for quantitative analysis, such as retrieving NMAX. The Channel A data for this period is useable.

4 Upcoming Work / Plan for Upcoming Releases

4.1 Level 1

Improved flatfield correction

Improve errors in geolocation

Correct spacecraft clock drift using ground receipt time

Updated geolocation correction (slit image movement)

Add wavelength dependent shape to scattered light background subtraction

Release of additional CHB data products

Quality flags for stars and moon in field of view

Quality flag for presence of xenon emission feature

4.2 Level 2

Release, where possible, of data held back in the current release due to artifacts or unresolved issues.

Better characterization of error components on retrieved geophysical parameters.

Apply additional spatial binning to the QEUV algorithm to reduce data scatter.

Implement bitwise DQI values for the ON2 and QEUV data products.

Implement an auroral boundary detection algorithm.

5 References

Ajello, J. M., Evans, J. S., Veibell, V., Malone, C. P., Holsclaw, G. M., Hoskins, A. C., et al. (2020). The UV spectrum of the Lyman-Birge-Hopfield band system of N2 induced by cascading from electron impact. Journal of Geophysical Research: Space Physics,125, e2019JA027546. https://doi.org/ 10.1029/2019JA027546.

McClintock, W. E., Richard W. Eastes, Alan C. Hoskins, Oswald H.W. Siegmund, Jason B. McPhate, Andrey Krywonos, Stanley C. Solomon, and Alan G. Burns, Global-scale Measurements of the Limb and Disk (GOLD) Mission Implementation: 1. Instrument Design and Early Flight Performance, *J. Geophys. Res. Space Physics*, *125*, e2020JA027797, https://doi:10.1029/2020JA027797, 2020.

McClintock, W. E., et al., Global-scale Measurements of the Limb and Disk (GOLD) Mission Implementation: 2. Observations, Data Pipeline and Level 1 Data Products, *J. Geophys. Res. Space Physics*, *125*, e2020JA027809, https://doi:10.1029/2020JA027809, 2020.

Saurav Aryal, J.S. Evans, R.W. Eastes, W. E. McClintock, J. Ajello (2021), N2 Lyman-Birge-Hopeld Band Vibrational Populations using GOLD Dayglow Measurements, In preparation.